

---

**This manuscript is a preprint and has not undergone peer-review. Please note that subsequent versions of this manuscript may have different content. If accepted, the final version of this manuscript will be available via the 'Peer-reviewed Publication DOI' link on the right-hand side of this webpage. Please feel free to contact any of the authors, we welcome feedback.**

---

## **Geomorphologic Controls on the Evolution of Submarine Channels in the Clifdenian-Tongaporutuan Interval of the Southern Taranaki Basin, offshore New Zealand.**

Dicky Harishidayat<sup>1\*</sup>, Chris Larsen<sup>2‡</sup>, Kamaldeen. O.L. Omosanya<sup>2</sup>

<sup>1</sup>Department of Geosciences, College of Petroleum Engineering and Geosciences, King Fahd University of Petroleum and Minerals, Dhahran.

<sup>2</sup>Department of Geoscience and Petroleum, Norwegian University of Science and Technology, Trondheim.

\*Corresponding author: Dicky Harishidayat ([dicky.hidayat@kfupm.edu.sa](mailto:dicky.hidayat@kfupm.edu.sa) or [dickyharishidayat@gmail.com](mailto:dickyharishidayat@gmail.com)).

‡Now Data Analyst at TINE Norway.

Twitter of Dicky Harishidayat @thearishidayat

Twitter of Kamaldeen Omosanya @extratectonics

### **Abstract**

The Clifdenian-Tongaporutuan interval in the Southern Taranaki Basin experienced significant turbidity activities during the Middle to Late Miocene leading to formation and burial of several submarine channels. The chronologic evolution of these channels is difficult to prove because of their architectures, repeated cut- and- fill, stacking patterns, erosive nature, and spatial-temporal interactions. In this study, mega merged high-quality 3D seismic reflection data (from three seismic surveys) coupled with five exploration industrial standard wellbore data were used to analyze the geomorphologic controls on the evolution of fourteen channels within the Clifdenian-Tongaporutuan interval (Middle to Late Miocene) of the southern Taranaki Basin. Our seismic geomorphological analysis (including seismic facies, slicing and seismic attributes techniques) shows that the channels belong to two main groups including isolated and amalgamated stacks, which can further include high sinuosity-meandering, low sinuosity-meandering, and straight channels. In addition, gamma-ray logs indicated cylindrical, bell and serrated stacking pattern of sandstone within thick shale interval that indicated the presence of submarine channels in the study area. Furthermore, the complicated spatial interactions of the channels (including architectural variation) and their temporal evolution reflects the activities of diverse turbidity flow regimes and a balance between waxing and waning energy phases. Importantly, the evolution, architecture and scale of the channel was influenced by eustatic sea-level fall in the late Waiauan at ca. 13 Ma, dominantly increased in clastic sediment supply (climate), palaeomorphology, and regional far-field stresses related to rifting and contraction in the Middle Miocene.

Keywords: Seismic geomorphology; architecture; seismic attributes; palaeoenvironment reconstruction; Miocene; Taranaki Basin; submarine channels; climate; turbidity current; sea-level, tectonic.

### **1.0 Introduction**

Submarine channels are primary conduits for transporting sediments into the deep marine area. In the last few decades, several integrated studies using 3D seismic reflection data, outcrop analogs, numerical modeling, and experimental modeling have enhanced our understanding of their evolution, architecture, size, and lithological composition (Abreu et al., 2003; Kneller, 2003; Posamentier and Kolla, 2003; McHargue et al., 2011; Peakall and Sumner, 2015). Architecturally,

submarine channels usually form a continuous spectrum of massive sand from erosionally confined, through a combination of erosion and constructional levees, to channels that are confined by levees, and with sinuosity varying from occasional bends in the channel to highly sinuous channels with numerous cut-off bends. These architectures are largely influenced by the initial erosive base, lateral stacking, lateral accretion, and sea-floor topography (Clark and Pickering, 1996; Mayall and Stewart, 2000; Deptuck et al., 2003; Kane et al., 2010; Pickering et al., 2015). In distal slope environments, submarine channels are more common where erosional and aggradational processes combine to form meandering systems (Abreu et al., 2003; Deptuck et al., 2003; Posamentier and Kolla, 2003; Mayall et al., 2006; McHargue et al., 2011).

Despite this knowledge on submarine channels, a lot more about their external morphologies, topologies, stacking pattern, and interaction with other elements of the submarine environments remain largely unknown because of (a) their similarities with submarine canyons (b) influence factors and (c) for the fact that the deepwater remains mysterious. For example, submarine channels share similar external morphologies with submarine canyons (Kneller, 2003; Kolla, 2007; Covault, 2011; Straub et al., 2012; Lemay et al., 2020; Harishidayat and Raja, 2022) and are commonly developed within and at the lower reaches of submarine canyons (Kuenen, 1953; Normark, 1978; Shepard, 1981; Stow and Mayall, 2000; Covault, 2011; Pickering and Hiscott, 2015; Fildani, 2017). The genesis and evolution of submarine channels also depend strongly on basin tectonics, flow behavior, climate, sea-level changes, and other factors that control the type, architecture, supply and deposition of sediment within channel belts (Kneller, 2003; Posamentier, 2003; Kolla, 2007; Covault, 2011; Peakall and Sumner, 2015; Fildani, 2017). Furthermore, seismic reflection data, which has offered many insights into the types and morphologies of most submarine channels are usually restricted to shallow and intermediate waters (Pettingill, 2004; Zhang et al., 2019; Weimer and Pettingill, 2020) where hydrocarbon exploration commonly takes place. Hence, the architecture, nature, and behavior of submarine channels in the deepwater environment (water depth: >200 m) is poorly known till date.

In this study, we offer new insights into (a) the seismic stratigraphic architecture and depositional elements of submarine channels, b) their spatial and temporal variability and c) multiple factors modulating their evolution and recurrence along continental margins. To achieve the aims of the study, a natural laboratory, the Southern Taranaki Basin, with a record of Neogene channels is used (Figure 1a). The distribution of submarine channels and their controlling factors in the study area are unexplored and poorly understood. Previous works in the study area concentrated on general stratigraphy and geology (e.g., Uruski, 2010; Campbell et al., 2012; Strogon et al., 2014; Uruski, 2015; Strogon et al., 2017; Higgs and King, 2018; Bull et al., 2019; Sahoo et al., 2020; Sutherland et al., 2020; Leila et al., 2022). Other works focused on the Middle Miocene deep-water sedimentary system (e.g., Baur et al., 2011; Kroeger et al., 2019), Late Miocene deep-water depositional system (e.g., Silver and Bedle, 2021), Plio-Pleistocene submarine channel (e.g., Mattos et al., 2019) and the Miocene to Pleistocene clinofolds succession (e.g., Franzel and Back, 2019). In more recent works from the study area, Li et al. (2017); Amonpantang et al. (2019); Lubo-Robles and Marfurt (2019) used artificial intelligence and machine learning to image channels in the Southern Taranaki Basin from seismic reflection data. In this study, we show the power of seismic geomorphologic methods at elucidating the concealed morphologies of these channels, their stacking patterns but most importantly their evolutionary histories. Importantly, a merged 3D full-stack seismic reflection data suite consisting of the Maui-Tui-Kokako data (Figure 1b), further offers an uncommon opportunity to investigate the spatial variability of these channels from the continental shelf into the deepwater environment.

## **2.0 Geological setting of the Taranaki Basin**

### **2.1 Tectonic evolution**

The study area is located within the Taranaki Basin on the Australian plate, off the eastern coast of New Zealand (Figure 1a). Along the eastern coast of New Zealand, a wide array of basins exists, the largest of them is the Taranaki Basin, which is located between the North and South Island (Figure 1a).

The Taranaki Basin covers an area of approximately 100,000 km<sup>2</sup> and it is filled by up to 9 km thick Cretaceous to Recent sediments (King and Thrasher, 1996; Uruski, 2015). In the Late Cretaceous, the Taranaki Basin evolved largely due to deformation zone associated with the present Australian–Pacific plate boundary (Knox, 1982; King and Thrasher, 1992; Campbell et al., 2012; Reilly et al., 2015; Uruski, 2015; Strogon et al., 2017). Multiple phases of basin evolution

are documented in the basin (King and Robinson, 1988; Mortimer, 2004; Reilly et al., 2015). These are Late Cretaceous (ca. 80 Ma) extensional phase during the opening of the Tasman Sea and breakup of Gondwana (Giba et al., 2012; Hemmings-Sykes, 2012; Mouslopoulou et al., 2012). A period of tectonic quiescence from the Early to Mid-Eocene (ca. 55 to 40 Ma) when subsidence associated with post-rift cooling of the crust resulted in marine transgression and development of a large embayment open to the Northwest (King and Thrasher, 1996; Strogon et al., 2014). The final but varied phase of basin evolution, which began with incipient shortening from ca. 43 to 40 Ma (Palmer and Andrews, 1993; Voggenreiter, 1993; Stagpoole and Nicol, 2008). Furthermore, contraction in the middle Eocene was characterized by reverse faulting and foreland basin development resulting in uplift and erosion of Late Cretaceous to Paleocene strata along the eastern margins of the basin (Stagpoole and Nicol, 2008). In the Late Oligocene to Early Miocene (25 to 20 Ma), shortening increased due to subduction of the Pacific Plate and displacement on the Alpine Fault (Knox, 1982; King and Thrasher, 1992; Kamp, 1999).

In the Southern Taranaki Basin, convergence inverted most of the original Late Cretaceous normal faults and further created new thrust faults while shortening in the northern and central parts of the basin was followed by extensional faulting related to intra-arc rifting associated with slab rollback or slab steepening at the Hikurangi subduction margin (Giba et al., 2010; Giba et al., 2013). At around 12 Ma, rifting started in the Northern Taranaki Basin, migrating southwards through time with the basin south of the Taranaki Peninsula accommodating extension since 3–4 Ma (King and Thrasher, 1996; Giba et al., 2010; Mouslopoulou et al., 2012).

## **2.2 Basin infill history**

In terms of basin fill, the Pakawau Group were deposited during the first phase of basin development and consists of terrestrial fluvio-lacustrine strata, interbedded with coal measures (Figures 2 and 3). These are essentially syn-rift sequences (2 to 3 km thick) filled into fault-bounded grabens and half graben structures (Palmer and Andrews, 1993; King, 2000; Campbell et al., 2012; Uruski, 2015; Strogon et al., 2017). The overlying Paleocene and Eocene deposits of the Kapuni and the Moa Groups constitute late-rift and post-rift, transgressive, terrestrial to marginal marine sequences (Palmer and Andrews, 1993; King, 2000; King et al., 2011; Higgs et al., 2012) that were deposited during rapid subsidence and a marine transgressive cycle (Figures 2 and 3). The accompanying shoreline fluctuation in the Early Eocene resulted in sequences of marginal marine and terrestrial deposits. Subsequently, thermal equilibrium was established towards the Oligocene resulting in a tectonically stable basin with little clastic sedimentary input. Tectonic quiescence and reduction in clastic sediment input during the Oligocene caused widespread deposition of limestones and calcareous mudstones of the Ngatoro Group (Otaraoa and Tikorangi Formations) throughout the basin (King et al., 2011). The transgressive phase reached its climax in the Early Miocene with deposition of the Taimana and Manganui Formations while the regressive phase started from the Mid-Miocene (Moki, Manganui, Mohakatino Formations) through the Pliocene (Giant Foreset Formation) to the present day (Higgs et al., 2012).

## **2.3 Middle to Late Miocene sands in the study area**

The oldest formation within the Middle to Late Miocene succession in the study area is the Manganui Formation (Figures 2 and 3) consisting of the Lower, Middle and Upper Manganui Formation (King and Thrasher, 1996; Campbell et al., 2012). Lithologically, the Manganui Formation is mudstone with significant amount of siltstone. Along the eastern boundary of the Taranaki Basin, concretion bands with thin strings of sandstone and limestone exists within the formation while along the central parts of the Taranaki Basin, the Lower Manganui Formation interfingers with the underlying Taimana Formation (King and Thrasher, 1996; King et al., 2011). In most parts of the basin, the Manganui Formation is overlain by the Moki Formation, which consists of sandstones of middle Miocene to Late Miocene age. Strata of the Moki Formation were deposited by gravity and turbidity flows in the mid to lower bathyal environment (Lock, 1985; Palmer and Andrews, 1993; Uruski, 2010). De Buck et al. (1991); De Buck (1994) proposed that the Moki formation consists of an elongated channel system running parallel to the slope in the north to northeast directions. Similarly, seismic data show that the sand units within the Moki Formation are also known as Sw, Sl/Sw or the Moki A that consists of sand units in turbidite complexes (Bushe et al., 2008; Grain, 2008; Strogon, 2011; Wunderlich and Kobstaedt, 2017). Additionally, the youngest Miocene interval, the Mount Messenger Formation is dominated by

basin floor fans and channel levee complexes deposited in fore-deep and intra (sub) continental Taranaki Basin.

### **3.0 Data and methods**

#### **3.1 Wellbore and 3D seismic reflection data**

A merged 3D seismic data consisting of three main seismic data (Maui-3D, Tui-3D, and Kokako-3D) was used in this study (Figure 1b). The seismic datasets were acquired within the central part of the Taranaki Basin, with the Kokako-3D stretching outwards into the northwestern platform of the Taranaki Basin (Figure 1). Bin sizes for the individual data are 25 x 12.5 m for both the Maui-3D and Kokako-3D, and 12.5 x 12.5 m for the Tui-3D survey. The merged seismic data is displayed in Society of Exploration Geophysicists (SEG) normal polarity with zero phase, where increasing in acoustic impedance is represent by positive amplitude or peak reflector. In contrary, decreasing in acoustic impedance is represent by negative amplitude or trough reflector. Additionally, the wellbore data used in this work are the Maui-1, Maui-3, Kahu-1, Tui-1, and Takapou-1 (Figures 1b and 3). Wireline logs available within the wells include resistivity, spontaneous potential, neutron, density, sonic, caliper, and gamma ray. Each of the wells also consists of a check shot survey. Moreover, biostratigraphic information was taken from the well completion reports and the newly revised framework of Roncaglia et al. (2013) to establish a lithostratigraphic framework for the interpreted horizons (Figures 2 and 3).

#### **3.2 Methods**

Seismic horizon interpretation involved mapping of six main horizons corresponding to the tops of the Moki Formation, lower Maganui Formation, Tikorangi Formation, 4th sequence lowstand, 5th sequence lowstand and Tt sand unit (Figures 2 to 4). The interpreted horizons and seismic amplitude were tied to the well tops and logs in all the available wells by creating synthetic seismogram of the seismic well-tie (Figure 3a). To interpret the channels in map view, volume attributes such as variance and sweetness were used. The variance attribute is a volume attribute that measures the similarity of waveforms over a given space (Chopra and Marfurt, 2007; Marfurt, 2015; Omosanya, 2020; Harishidayat et al., 2022). Variance is a good seismic attribute for identifying sharp changes in seismic reflection patterns related to faults or margins of submarine channels (Chen and Sidney, 1997; Chopra and Marfurt, 2007; Pigott et al., 2013). The variance attribute was used extensively for interpreting the channels and their evolution in vertical or seismic sections. The sweetness attribute is useful for differentiating shale from sand deposits and for interpreting submarine channels (Hart, 2008; Li et al., 2017). As shale or hemipelagic sediments typically have low acoustic impedance, they are usually reflected as low amplitude reflections, or multiple stacks of high-frequency reflections while sands are characterized by high acoustic impedance, and low-frequency reflections (Hart, 2008; Sena et al., 2011; Li et al., 2017). The sweetness attribute is calculated by dividing the instantaneous amplitude (amplitude envelope) by the square root of the instantaneous frequency (Chopra and Marfurt, 2007). Sands typically have higher sweetness values than shale albeit the sweetness attribute is sensitive to thin layers of alternating shale and sand due to destructive interference of seismic signals (Hart, 2008; Sena et al., 2011).

To map the channels in their geomorphologic or depositional state, the approach of strata slicing was adopted from Zeng (2010), where the stratal or proportional slicing technique creates several evenly spaced time-slices that conforms to the desired interval. For any interval containing channels, the upper and lower boundaries were established and interpreted in a seeded grid, which were converted to structural maps. Furthermore, flattened seismic cubes were made using the structural maps as input and stratal slices obtained in a window of ca. 20 ms above the flattened base boundaries. The stratal slices were made from both the variance and sweetness seismic attributes. Once the spatial extents of the channels were mapped in time slices, the geomorphologic features identified in map were then validated on seismic profiles following established submarine channel facies and sequence stratigraphic schemes proposed by Abreu et al. (2003); Posamentier and Kolla (2003); Mayall et al. (2006); Harishidayat et al. (2018); Niyazi et al. (2018); Harishidayat and Raja (2022).

In addition, stacking pattern interpretation of gamma ray from available wellbore was utilized to support channels interpretation from 3D seismic reflection data (Figures 3b to 3d) using the classification scheme of Rider (1986); Asquith et al. (2004) where gamma ray response is a proxy

for grain size that represent radioactive minerals in organic matter. Therefore, depositional elements and sedimentary processes could be interpretable.

## 4.0 Results

### 4.1 Seismic stratigraphic architecture and depositional elements

The first three sequences (1 to 3) interpreted by Wunderlich and Kobstaedt (2017) do not contain channels and have been interpreted here in order to determine the relative age and position of the channels within the regional geologic context. Fourteen (14) channels are interpreted in this study and they are part of Sequence 4 and 5 of Kroeger et al. (2019).

In terms of stratigraphic framework, Sequence 1 is Mid Clifdenian (Sc) to Early/Mid Liburnian (Sl) in age (Figure 2). The base of the sequence is marked by a dramatic shift in the gamma ray log response from upward increasing trend to a drop-in gamma ray log response (Figure 3a). Sequence 1 progressively thins basinward, being ca. 165 m in the Maui-1 well and around Maui-3 region to being ca. 100 m in the central area around Kahu-1 and Tui-1, and to becoming ca. 35 m thick in well Takapou-1 (Figure 3a). Lithologically, Sequence 1 is dominated by interbedded sandstone, silt or mudstone and on seismic profiles it is represented as low amplitude seismic reflections (Figure 4). Sequence 2 is part of the Moki Formation and dated middle to Late Liburnian (Sl). Log character of this sequence includes blocky gamma ray signature that is intercalated by spikes (Figure 3). Sequence 2 is ca. 140 m thick in Maui-1 and Maui-3, ca. 35 m in Tui-1 and Kahu-1, and ca. 25 m in Takapou-1 (Figure 3a). The blocky signature of the gamma ray logs and spikes indicate well-developed sandstone interlayered by mud-rich intervals. Seismic expression of Sequence 2 includes moderate amplitude and semi-continuous reflections, whereas its base consist of high amplitude regional reflector corresponding to the Maari shale (Figure 4).

Sequence 3 is Late to Latest Liburnian (Sl) in well Maui-1 and Maui-3; Mid to Late Liburnian (Sl) in Tui-1; and Late Liburnian (Sl) to Early Waiauan (Sw) in Takapou-1 (Figure 2). The gamma ray log response through sequence 3 is bell-shaped (Figures 3a and 3d), indicating an upward fining sequence analogous to amalgamated sand deposits. The thickness of the lower part of Sequence 3 is ca. 30 m in Maui-1 and Maui-3; 20 m in Tui-1 and Kahu-1; and 10 m in well Takapou-1, respectively (Figure 3a). The upper part of sequence 3 is characterized by a high gamma ray value, with frequent low gamma ray spikes indicative of mud-rich sediments interfingering by sandstones in the distal part of the basin (Figure 3). The upper part can reach up to 55 m in Maui-1 and Maui-3; ca. 45 m in Tui-1 and Kahu-1; and ca. 15 m in Takapou-1 (Figure 3). Seismic facies of sequence 3 include moderate to high amplitude reflections at the base close to the Maari Shale and moderately high amplitude reflections at the upper part (Figure 4).

Sequence 4 is in the middle part of the Manganui Formation and consists of several Sw sand intervals in wells Maui-1 and Maui-3 (Figure 3). In well Kahu-1 and Tui-1, sequence 4 has its base in the middle Manganui Formation and its top at a thick sandstone deposit, informally named Tt sands. Well Tui-1 also includes a unit of Sw sands within this sequence (Figure 3). The sequence within the Takapou-1 well includes a Sw sand unit and its upper boundary is capped by the Sw/Tt sand unit (Figures 2 to 4). Sequence 4 is late Liburnian to the late Waiauan in wells Maui-1 and Maui-3, and occur until the transition between the Waiauan and Tongaporutuan in the Tui-1 and Takapou-1 wells (Figures 2 and 3). Lithologically, the sequence is dominated by mudstone as shown by the high gamma ray values in wells Maui-1 and Maui-3 and with some individual sand units (Figure 3). On seismic profiles, the lower part of sequence 4 includes medium to low amplitude, semi-continuous reflections while its upper part shows higher amplitude continuous reflections that can be regionally mapped (Figure 4).

The youngest sequence in this study is sequence 5, which has its base as the Sw sands in well Maui-1 and Maui-3, at a thick Tt sand in Kahu-1 and Tui-1 wells, and at Sw/Tt in the Takapou-1 well (Figure 3). The Sw/Tt sand unit is correlated to the Tt sand unit in Tui-1 and Kahu-1 wells and has been informally referred to as Tt sand 1 and 2 (Roncaglia et al., 2013). In this work, the name Tt sand is used to describe the lower sands within sequence 5 while Sl/Sw sand is used for older sand units (Figure 3). Sequence 5 is early Tongaporutuan in age and consist of all the submarine channels described in this work. The gamma ray signature across sequence 5 is overall blocky in both the Kahu-1 and Tui-1 wells, while the Takapou-1 well shows a more spiked expression. In the Maui-1 and Maui-3 wells, the gamma ray value for sequence 5 is entirely low

(Figure 3) whereas seismic facies of sequence 5 includes continuous and high amplitude reflections (Figure 4).

## 4.2 Submarine channels in the study area

Fourteen (14) submarine channels (Channels A to N) were interpreted from the merged 3D seismic data with emphasis on their chronological order, facies, stacking pattern, sinuosity, and their architectural elements (Figures 4 to 8). An overview map of the interpreted channels is provided in Figure 8, which shows that most of the channels are oriented in the NW-direction, except for channel A and N that trend in the North direction. Based on their vertical and horizontal interaction with other channels, the channels are grouped into (a) amalgamated (channels E-F, K-L, G-H and N-M) and (b) isolated types (channels A, B, C, D, I and J). Their map view geometries shows that the channels can further be subdivided into meandering channel (channels A, D, E, F, J, L, G, H, N and M) and straight channel (channels B, C, I and J) types.

### 4.2.1 Isolated channels

#### Channel A

Channel A is a meandering channel that is interpreted to be the latest active channel within a channel complex because it does not show any incision into the Moki Formation (Figures 5a to 5d). Channel A is characterized by two separate elements CD:A and CD:B. Both elements show high amplitude reflections at their bases and tops albeit CD:A is flanked by low amplitude levees on its sides (Figures 5a and 5b). In seismic profiles, CD:A shows little or no signs of vertical aggradation (Figure 5). In the kokako survey, Channel A is confined by erosional walls (Figure 5), and characterized by an erosional terrace (ET) and lateral accretion packages (LAPs). In map view, the continuous meandering nature of the channel is associated with several abandoned meandering loops and channel segments (Figures 8 and 9). The older abandoned segments and meandering loops often show high amplitude, which are interpreted to be sandy over-bank deposits (Figure 5b). Before the braided pattern, the channel shows some signs of channel amalgamation (Figure 9).

#### Channel B

The lower part of this channel complex shows sinuous channels that crosscutting each other, while the overall shape of the channel complex is relatively straight (Figures 7, 8 and 10). Slumped deposits were interpreted along the upper part and erosional walls of the channel. In seismic profile (Figures 7 and 10), Channel B shows high amplitude reflections with varying degree of intensity at its base. These reflections fill the channel belt and were interpreted as amalgamated channel or lag deposits. Channel B also shows no aggradation and is flanked by a layer of continuous high amplitude reflections, which are sheet sand deposits (Figure 7). The sheet sand deposits are part of the informal Sl/Sw sand unit (Figures 2 and 3).

#### Channel C

Channel C shows overall low sinuosity, channel cross-cutting, and meandering pattern in the Maui-3D seismic survey area (Figures 8 and 11). In this part, individual meandering loops can be identified while in the Tui-3D seismic survey area, the channel has significantly lower sinuosity. In seismic profiles, Channel C is characterized by steep erosional walls, a minor normal fault at its southeastern wall, and deep cutting into the Manganui Formation (Figure 6). A series of discontinuous high amplitude reflections are found at the base of the channel and along the southeastern channel wall. These deposits are reflected as high and low amplitude reflections and interpreted as amalgamated crosscutting channels with deposits ranging from lag deposits to amalgamated channel sand deposits (Figure 6). In distal areas, Channel C shows lower erosional walls and the channel cuts down into the underlying continuous moderate amplitude reflections of the Moki Formation (Figures 6 and 11). In these areas, the channels also have amalgamated channel sand deposits at its base and an erosional terrace formed as an abandoned meandering loop (Figures 6 and 11). The seismic facies of this terrace are reflection-free to low amplitude, indicating homogeneous or fine-grained over-bank deposits.

#### Channel D

Channel D is a highly sinuous channel with multiple abandoned meandering loops (Figures 6 and 7). This meandering interval is best expressed in the first two-thirds of the Maui-3D seismic survey area while in the other, the channel is straight (Figures 8 and 12). The sweetness slice shows a large variation in amplitude for the channel signifying the presence of a mix of depositional

materials within the channel (Figure 12b). In seismic profile, Channel D is incised into a unit of continuous low amplitude reflectors in the Manganui Formation (Figures 4, 6 and 7). On the flank of the channel are continuous and high amplitude reflectors while the base of the channel shows semi-continuous and high amplitude reflections, with dipping low amplitude reflectors covering them. The upper part of the channel shows low amplitude semi-continuous reflectors interpreted as passive infill after the channel was abandoned (Figures 6 and 7).

#### Channel M

Channel M is characterized by large erosional walls with slump deposits and several abandoned meandering loops and erosional terraces (Figure 6). Channel M is associated with uniform and high amplitude within the channel belt, an infill of low amplitude reflections, and high amplitude reflections in the abandoned meandering loops (Figures 6 and 13). Additionally, Channel M incised down into a unit of continuous and high amplitude reflections of the Tt sand unit (Figure 6). The base of the channel shows discontinuous high amplitude reflectors, with a slight V-shaped area in the middle where low amplitude reflections are predominant. A second channel within the erosional confines of channel M, Channel M2, show high discontinuous amplitude reflectors at its base. At its northeastern flank, continuous and high amplitude reflections exists, which are over-bank deposits from channel M2 covering the passive infill of channel M.

#### Channel N

Channel N is a highly sinuous channel situated on top of channel M (Figures 6 and 8). In map view, Channel N shows inner channel bends i.e., point bar deposits (Figure 13) while the base of the channel shows discontinuous high amplitude reflections, which migrate laterally and vertically from the center towards the northeast (Figures 6 and 13). These reflections are further interpreted as channel deposits from; (1N) an early cross-cutting and amalgamating phase; (2N) transition to a more aggradational phase with organized channel stacking pattern; and (3N) a highly aggradational phase with organized channel stacking pattern (Figures 6 and 8). Moreover, Channel N is flanked by continuous to semi-continuous and moderate amplitude reflections (external levee deposits) that are dipping away from the channel (Figures 6 and 13). Reflections dipping towards the migrating channel deposits of channel N are internal levee deposits, supporting channel aggradation (Figures 6 and 13). In addition, stacking pattern of the gamma ray log response of this Channel N on Tui-1 wellbore indicated fining upward pattern of sandstone deposit (Figure 3d).

### 4.2.2 Amalgamated stacks

#### Channels E and F

Channels E and F stratigraphically lie above channel D within the Manganui Formation (Figures 7 and 8). In the variance stratal slice (Figure 14), a clear separation between the two channels can be observed as Channel E follow almost the same path as Channel D while in seismic profiles, Channel F show significant channel downcutting and amalgamation in its lower part, with a phase of increased meandering taking over towards the end (Figures 7, 8 and 14). The seismic profile in Figure 7 shows that the base of channel F includes discontinuous and high amplitude reflections (1F). Above this, an interval of continuous, mainly high amplitude reflections is interpreted as internal levees supporting channel aggradation. A unit of aggradation channels (2F) is also interpreted in a set of discontinuous and moderate amplitude reflections while the unit marked 3F shows semi-continuous and high amplitude reflections, and an area that appears W-shaped with moderate amplitude reflections (Figures 4 and 7). This is interpreted as a laterally migrating and aggravating channel. Above this unit, internal levees with moderate to high amplitude reflections are observed while along the eastern walls of Channel F, there is a series of discontinuous and high amplitude reflections interpreted as vertically migrating channel deposits (Figure 7). The continuous and high amplitude reflections on the flanks of Channel F are also interpreted as lobe deposits, which are overlain by a small unit of continuous, dipping, and low amplitude reflections or levee deposits. In Figure 7, the distinction between Channel E and F becomes less clear as the area marked as 2 show a continuous and high amplitude reflection interpreted as the erosional base of Channel F. Above this, are several discontinuous and high amplitude reflections (3) and (4) analogous to cross-cutting and amalgamating channels. The dipping reflection (5) is interpreted as a laterally and aggrading channel (Figure 7). In figures 7 and 14, Channel F is flanked by continuous and high amplitude reflections that are the lobe of channel D. The upper unit of these lobe deposits can also be correlated to the Tt sand in well Tui-1. On top of this lobe deposit, are levee deposits that dip away from the channel belt (Figure 7).

## Channels K and L

Channel K is the younger subset of channel KL. These two channels merged after the Cape Edgemont Fault in the Maui-3D seismic survey area and were both interpreted in the Maui-3D and Tui-3D seismic survey areas (Figures 8 and 14). Moreover, channel KL crosses the Whitki reverse fault without any alteration in form or direction suggesting that the fault was not active at the time the channel was formed (Figures 8 and 14). In map view, channel KL show channel cross-cutting and amalgamation character within and between the channels K and L. Furthermore, both channel K and L show signs of poor confinement in stratal slices (Figure 14). Architectural elements associated with Channel L include a crevasse splay, slump deposits, lateral accretion packages, laterally migrating and aggrading channel deposits, internal levees, over-bank deposits, and passive channel infill (Figures 4 and 7). In addition, stacking pattern of the gamma ray log response of this Channel L on Kahu-1 wellbore indicated cylindrical or blocky pattern of sandstone deposit (Figure 3c).

## Channels G and H

Channels G and H are both interpreted after the Cape Edgemont Fault in the Maui-3D seismic survey area, and these two channels merged shortly after the fault into channel GH (Figures 6, 8 and 15). Figure 6 shows that both channels G and H are incised into a unit of high amplitude reflections or lobe of channel D lobe and overbank/levee deposits of Channel F. The base of Channel H (1H) is characterized by semi-continuous and high amplitude reflections. On the southeastern flank of Channel H, levee deposits are interpreted as continuous, parallel, and moderate amplitude reflections. Overlying these reflections are parallel, semi-continuous, and moderate amplitude while discontinuous, and medium to high amplitude reflections are observed in the central and northwestern part (2H) and (3H). These reflections correspond to channel aggradation with supporting internal levees and profound stacking patterns (Figures 4, 6 and 15).

## Channels I and J

Channel I is a minor straight channel that is interpreted in the Maui-3D seismic study area after the Cape Edgemont Fault. The channel exits the study area to the east and lies above Channel B (Figures 6, 7, 8 and 16). Internal architecture of Channel I include discontinuous and high amplitude reflections corresponding to channel deposits (Figures 4 and 7). The channel deposits show high amplitude reflections on the sweetness slide that may signify the presence coarse-grain sediments (Figures 7 and 16). On the flanks of Channel I, the seismic amplitude is characterized by semi-continuous and high amplitude reflections with over-bank deposits belonging to the Sl/Sw sands (Figure 7). Channel J is a sinuous channel interpreted in both the Maui-3D seismic survey after the Cape Edgemont Fault and in the Tui-3D seismic survey (Figures 8 and 16). In map view, Channel J is straight and narrows until it crosses the Whitki reverse fault. After this fault, the channel shows much more sinuosity until it ended up within the confines of channel C (Figures 8 and 16). Channel J lies within a unit of low amplitude reflections correlated to the Manganui Formation (Figures 4 and 7). The base of the channel and its infill show discontinuous and high amplitude reflections or lateral accretion package (Figures 4 and 7). Channel J is also flanked by semi-continuous and moderate amplitude reflections interpreted as levee deposits (Figure 7). These levees overlie semi-continuous and high amplitude reflections that are either the result of the lithological contrast between the levees and the underlying Manganui Formation or by overbank deposits from channel I.

## 5.0 Discussion

### 5.1 Temporal and spatial evolution of the channel systems

A timeline showing the temporal evolution of the interpreted submarine channels is shown in Figure 17. Following the deposition of the lower Manganui Formation, Channel C was eroded into the lower Manganui Formation. This is evidenced by the undercutting of the lower Manganui Formation as observed in both seismic sections and time maps (Figures X and X). The erosional nature of Channel C is further revealed by the presence of channels walls cutting into the Manganui Formation in less sinuous pattern with high angle topography (Figure 18). Subsequently, Channel D eroded into the Tt sand unit while further depositing some Tt sands as channelized lobe and minor levee. In this study, Channel D is interpreted as a channelized lobe complex (Figures 8 and 12). Channel M further eroded into the Tt sand unit and deposited minor levee deposits on the flanks with more sinuous pattern and low angle topography (Figure 18). Channel M is younger than Channel C as it is cut into Channel C. Then, channels J, K, and L in that order, eroded down into the Tt sand unit and ended up following the confines of Channel C. The channel above, 'F' was associated with significant over-bank/levee deposits as it cut into

channels J, K, and L, and was filled with sand-rich deposits (Figure 14). This was followed by the deposition of the debris flow deposit marked X (Figure 6). Strata of X were deposited over the levee of Channel M, in the northeast, and in the distal part of the study area where it overlies the levee or over-bank deposits of Channel F (Figures 6 and 7). Channel G, H, and their levee deposits were formed afterwards with low angle topography (Figure 18) and their deposits were later covered by the levee deposits of Channel N (Figure 6). Hence, in terms of relative age and order of formation, Channel N is interpreted as the youngest channel while Channel A is interpreted as the oldest channel in the study area. Channel B bears several similarities with Channel C and are interpreted to be of the same age. Deposits of Channel E are infilled above Channel D and crosscut by Channel F making its interpretation cumbersome. Similarly, Channel I is interpreted to have formed before Channel J as Channel J is observed to crosscut it. Laterally, channels B, C, EF, and IJ are developed in relatively high angle topography that created less sinuosity pattern (Figure 18). Whereas, channels G, D, H, KL, M, A and N are having more sinuosity pattern related to low angle topography (Figure 18).

Furthermore, high amplitude reflections are common with sandy deposits, especially at lithological contrast. When these reflections are continuous, they often show either frontal or crevasse splay (Posamentier and Kolla, 2003). When they are discontinuous, the reflections indicate channel sand deposits. With submarine channels especially turbidite channels, repeated lateral and vertical migration is common. Vertical stacking is more predominant than lateral one (Abreu et al., 2003; Posamentier and Kolla, 2003) and are usually linked to erosional surfaces (Jobe et al., 2011). On the other hand, low amplitude reflections are common with fine-grained sediments especially parallel and subparallel continuous reflections of channel levees, while discontinuous and dipping reflections might show lateral accretion (Abreu et al., 2003; Posamentier and Kolla, 2003; Harishidayat et al., 2018). Moreover, chaotic seismic reflections within the channel belts are analogous to debris flow or mass transport deposits resulting from the collapse of the channel walls (Mayall and Stewart, 2000; Posamentier and Kolla, 2003).

## 5.2 Depositional model

The interpreted evolution stages of the channels within the framework of sequence stratigraphy (a) erosion and sediment bypass, (b) channel amalgamation and low aggradation, (c) disorganized channel stacking pattern and moderate aggradation, and (d) organized channel stacking pattern and high aggradation. The proposed timeline (Figure 17) shows a clear progression from channels dominated by their waxing phases to those channels with more significant waning phases. This timeline further highlights that the basin experienced a sequence-scale waxing to waning shift, related to eustatic change from lowstand towards highstand at the beginning of the Tongaporutuan stage. The eustatic curves from Kominz et al. (2008); Zachos et al. (2008); John et al. (2011); Kroeger et al. (2019); Miller et al. (2020) show increasing sea-level around 11 Ma (Figure 2). This coincides with the beginning of the Tongaporutuan stage and the deposition of the Tt sand unit in the Tui-3D and Kokako-3D seismic survey area Figure 17. Strata deposited during this stage are lowstand sequences. In the Maui-3D seismic survey area (Figures 1b and 8), this sequence is dated the late Waiauian (Roncaglia et al., 2013; Kroeger et al., 2019). Hence, Channels B and C along with the Sw sand over-bank deposits of Channel B are the earliest channels interpreted within this sequence (Figure 17). Based on its geometry, channel complex B have been interpreted to be the distal part of a sand-rich channel complex deposited during a lowstand system.

The transition to lowstand resulted in the deposition of the Tt sand and the Sw sands in the Maui-3D seismic survey and in the turbidity flows becoming sand-rich and having greater waxing energy. After the Tt sands was deposited by Channel D, the basin was incised by several channels (e.g., M, I, J, K and L) with significant waxing energy (Figures 3, 9 and 14). These channels are markers of a system moving away from lowstand setting (Posamentier and Kolla, 2003; McHargue et al., 2011). The deposition of the debris flow deposit X marked a stage of slope disequilibrium brought on by significant sea-level change (Posamentier and Kolla, 2003). And with further deposition of the Tt sand by Channel F, the sequence reverted to lowstand. Moreover, Channels F, G, H, and N show significant signs of waning phase that signifies a shift in the prevailing trend of aggressively waxing turbidity flows to waning flows. This is chiefly true for Channel N, which shows limited signs of stage 3, indicating mud rich turbidity flows and cessation of the lowstand system tract (Posamentier and Kolla, 2003; McHargue et al., 2011). The model presented above is consistent with the idealized example proposed by Posamentier and Kolla (2003) where a unit of debris-flow deposits is often overlain by frontal splay deposit, levee deposits, debris flow deposits again and then capped by a condensed deposit of hemipelagic or

pelagic deposits. A similar predictive model is observed in the study area where an underlying lobe complex is overlain with leveed channels that in turn have debris flow deposited in the distal parts of the levees. This is typical of deep-water sequence albeit with a higher complexity than the one presented by (Posamentier and Kolla, 2003).

The lateral shifting and vertically aggrading channel patterns were occurred in the channel development of the study area. These indicated by stacking pattern of the channels; channels A, G and H are shifted laterally whereas channels B, C, D, E, F, J, K, L M and N are aggraded vertically (Figures 5, 6, 7 and 19). This lateral shifting is part of channel avulsion or bend cut-off (Abreu et al., 2003; Kolla, 2007), rising the equilibrium profile in the waning phase (McHargue et al., 2011), when the base of the channel system is at grade with the equilibrium profile (Hodgson et al., 2011) and the helical flow in the channel system (Dykstra and Kneller, 2009). In addition, lateral shifting of the channel system indicates increased organization of component channels that erode external flank and widen the channels surface (Abreu et al., 2003; Hodgson et al., 2011; McHargue et al., 2011; Hansen et al., 2017). Furthermore, the vertically aggrading channels complexes in the study area is represented by cross-cutting channels in relatively vertical direction (Figures 5 to 7). Once the channel equilibrium profile continues to rise (substantial increase in slope accommodation), the submarine channel starts to aggraded in a vertical direction with no significant lateral offset of depositional facies (Kneller, 2003; Hodgson et al., 2011; McHargue et al., 2011). The relative directions and styles of facies heterogeneity (correspond to the position, depth and thalweg orientation) are contributed to the lateral shifting and vertical aggrading channel patterns and fill architecture (Brunt and McCaffrey, 2007). On an all, the geomorphology of submarine channels has also influencing by local factors in this continental slope environments (e.g., submarine wall's collapse, different maturity of turbidite flows, slope accommodation, etc.).

### **5.3 Regional tectonic and secondary factors controlling recurrence of channels**

Tectonic uplift in the Taranaki Basin is proposed as the main driver of changes in channels lateral and vertical stacking pattern (Reilly et al., 2015; Bull et al., 2019; Franzel and Back, 2019). Evidence of channel-faults interaction within the study interval is highlighted in (a) location of channels on the footwall of the Cape Edgemont fault, which evolved initially as a normal fault and (b) interaction of some of the channels with the Whitiki reverse fault (Figures 8, 19 and 20). These observations suggest that the evolution of the channels was impacted by tectonics and provide evidence that the faults were probably active during the deposition of sediments preserved within sequence 5 and the channels. According to Reilly et al. (2015), the Cape Edgemont fault is linked to contractional deformation in Late Miocene (ca. 11-5.5 Ma), pointing to a change from its initial extensional style and the contribution of tectonics to the creation of accommodation space. This change in deformation style appears to have impacted regional basin infill styles especially the deposition of sediments in local depocenters in its footwall and further northwest of it by channels.

Although, previous studies (e.g., (Reilly et al., 2015) proposed that intra-basinal faults such as the Cape Edgemont and Whitiki faults have limited impacts on basin infill as sedimentation rates surpassed displacement rates on the faults between ca. 14-7 Ma. Nevertheless, the dominant northwest orientation of most of the channels and the north orientation of Channels A and N (Figures 8 and 20) show that the sediments were derived from areas to the south and southeast of the study area, which is the location of present-day South Island. Hence, sediment transport from the S and SE can be linked to high elevation or tectonic uplift in these areas and on a regional scale to enhanced convergence of the Australian and Pacific plates during the deposition of sequences 5 (Figures 1 and 20). Hinterland uplift could have resulted in increased gradient and accommodation space basinward, favoring deposition of sediments arriving from the south via the channel systems. Moreover, the Surville and Waimea-Flaxmore fault system, to the south of the study area are likely to have contributed to focusing clastic sediments northward for onward delivery to the Southern Taranaki Basin via deepwater channel systems (Bull et al., 2019). Moreover, changes in channels' orientation from dominant NW to N could also reflect the impact of other factors such as basin gradient and shelf propagation.

As the channel exits the study area (Figures 1b, 8 and 9), its element appears to widen and take on a braided pattern, signifying a transition from channel to frontal splay due to a sharp gradient change. Variation in basin gradient may dictate the location of depocenters near the shelf-slope system, which in turn may be linked to changes in the direction of shelf progradation. Bull et al. (2019) show that the northwest orientation of Southern Taranaki Basin channels in the Middle to Late Miocene parallels the direction of shelf progradation. Therefore, it is suggested that changes

in channels orientation coupled with their varied sinuosity may reflect dynamic changes in sediment supply patterns into the Southern Taranaki Basin in the Tortonian, rate of hinterland uplift, and impact of regional far field stresses related to plate reorganization.

## **6.0 Conclusions**

This study investigated the geomorphological evolution of 14 submarine channels with the Clifdenian to the Early Tongaporutuan interval (Middle to Late Miocene) of the Southern Taranaki Basin, New Zealand using combination of conventional seismic facies analysis, multiple seismic attribute analyses and slicing technique. The data and approach used here allowed the internal architecture and external elements of the submarine channels to be deciphered and interpreted. The chronological and depositional models shows that changes in eustatic sea-level was a major controlling factor during the evolution of the channels. After the lowstand during the deposition of the Moki Formation at ca. late Lillburnian (ca. 15 Ma), the study area experienced only minor turbidity activity until the late Waiauan (ca. 13 Ma) when sea-level fall promoted significant incisions of the substrate by turbidity currents. Highly erosive submarine channels created deeply incised valleys into the continental slope, while thin sheets of sands were deposited as the Sw sand units. With the lowstand system tract being stabilized, Tt sand was deposited as channel lobes. Importantly, the varied changes in channels orientation reflect the impact of sediment supply patterns into the Southern Taranaki Basin in the Tortonian, rate of hinterland uplift, and impact of regional far field stresses related to reorganization of the Australian and Pacific Plates in the Miocene.

## **Acknowledgements**

The authors thank New Zealand Government for allowing to access the data through New Zealand Petroleum and Mineral database. Schlumberger for PETREL Software donate to Department of Geosciences and Petroleum - Norwegian University of Science and Technology as well as Department of Geosciences - College of Petroleum Engineering and Geosciences - King Fahd University of Petroleum and Minerals. We acknowledge the insights and efforts of journal editor and reviewers that improved the quality of the manuscript. This work is based upon the 2<sup>nd</sup> author MSc thesis at the Department of Geosciences and Petroleum - Norwegian University of Science and Technology.

## **Conflict of interest**

The authors have no conflict of interest to declare.

## **Data Availability Statement**

The data that support the findings of this study are available publicly in the New Zealand Petroleum and Mineral database website.

## **References**

- Abreu, V., Sullivan, M., Pirmez, C., Mohrig, D., 2003. Lateral accretion packages (LAPs): an important reservoir element in deep water sinuous channels. *Marine and Petroleum Geology* 20, 631-648.
- Amonpantang, P., Bedle, H., Wu, J., 2019. Multiattribute analysis for channel element discrimination in the Taranaki Basin, offshore New Zealand. *Interpretation* 7, SC45-SC61.
- Asquith, G., Krygowski, D., Henderson, S., Hurley, N., 2004. *Basic well log analysis*. American Association of Petroleum Geologists.
- Baur, J.R., King, P.R., Stern, T., Leitner, B., 2011. Development and seismic geomorphology of a Miocene slope channel megasystem, Offshore Taranaki Basin, New Zealand, *Seismic Imaging of Depositional and Geomorphic Systems: 30th Annual Research Conference Proceedings*, Houston, Society of Economic Palaeontologists and Mineralogists, pp. 618-649.
- Bull, S., Nicol, A., Strogon, D., Kroeger, K.F., Seebeck, H.S., 2019. Tectonic controls on Miocene sedimentation in the Southern Taranaki Basin and implications for New Zealand plate boundary deformation. *Basin Research* 31, 253-273.

- Bushe, H., Baur, J.R., Arnot, M.J., Jones, C., King, P.R., Leitner, B., Massey, M., Milner, M., Morgans, H.E.G., Roncaglia, L., Zhu, H., 2008. Mapping and visualisation of midmiocene channel systems in the kupe region, New Zealand Petroleum Conference Proceedings.
- Campbell, H., Malahoff, A., Browne, G., Graham, I., Sutherland, R., 2012. New Zealand Geology. Episodes 35, 57-71.
- Chen, Q., Sidney, S., 1997. Seismic attribute technology for reservoir forecasting and monitoring. The Leading Edge 16, 445-448.
- Chopra, S., Marfurt, K.J., 2007. Seismic attributes for prospect identification and reservoir characterization. SEG Geophysical Development Series.
- Clark, J.D., Pickering, K.T., 1996. Architectural elements and growth patterns of submarine channels: application to hydrocarbon exploration. AAPG bulletin 80, 194-220.
- Covault, J.A., 2011. Submarine fans and canyon-channel systems: a review of processes, products, and models. Nature Education Knowledge 3 (10), 4.
- De Buck, J.E., 1994. Moki formation, a miocene reservoir sequence, its facies distribution and source in offshore, southern taranaki basin, New Zealand. Petroleum Report Series PR1800. Ministry of Economic Development. The Government of New Zealand.
- De Buck, J.E., Perry, S., Webby, D., Goodin, B., 1991. Appraisal of the maui-4 and moki-1 oil discoveries PML38144 and PML38145, New Zealand Petroleum Conference Proceedings, pp. 155-167.
- Deptuck, M.E., Steffens, G.S., Barton, M., Pirmez, C., 2003. Architecture and evolution of upper fan channel-belts on the Niger Delta slope and in the Arabian Sea. Marine and Petroleum Geology 20, 649-676.
- Fildani, A., 2017. Submarine Canyons: A brief review looking forward. Geology 45, 383-384.
- Franzel, M., Back, S., 2019. Three-dimensional seismic sedimentology and stratigraphic architecture of prograding clinoforms, central Taranaki Basin, New Zealand. International Journal of Earth Sciences 108, 475-496.
- Giba, M., Nicol, A., Walsh, J.J., 2010. Evolution of faulting and volcanism in a back-arc basin and its implications for subduction processes. Tectonics 29.
- Giba, M., Walsh, J.J., Nicol, A., 2012. Segmentation and growth of an obliquely reactivated normal fault. Journal of Structural Geology 39, 253-267.
- Giba, M., Walsh, J.J., Nicol, A., Mouslopoulou, V., Seebeck, H., 2013. Investigation of the spatio-temporal relationship between normal faulting and arc volcanism on million-year time scales. Journal of the Geological Society 170, 951-962.
- Grain, S.L., 2008. MSc Thesis: Palaeogeography of a mid miocene turbidite complex, Moki formation, Taranaki basin, New Zealand. Victoria University of Wellington.
- Hansen, L., Janocko, M., Kane, I., Kneller, B., 2017. Submarine channel evolution, terrace development, and preservation of intra-channel thin-bedded turbidites: Mahin and Avon channels, offshore Nigeria. Marine Geology 383, 146-167.
- Harishidayat, D., Farouk, S., Abioui, M., Aziz, O.A., 2022. Subsurface Fluid Flow Feature as Hydrocarbon Indicator in the Alamein Basin, Onshore Egypt; Seismic Attribute Perspective. Energies 15, 3048.
- Harishidayat, D., Omosanya, K.O., Johansen, S.E., Eruteya, O.E., Niyazi, Y., 2018. Morphometric analysis of sediment conduits on a bathymetric high: Implications for palaeoenvironment and hydrocarbon prospectivity. Basin Research 30, 1015-1041.

- Harishidayat, D., Raja, W.R., 2022. Quantitative Seismic Geomorphology of Four Different Types of the Continental Slope Channel Complexes in the Canterbury Basin, New Zealand. *Applied Sciences* 12, 4386.
- Hart, B.S., 2008. Channel detection in 3-D seismic data using sweetness. *AAPG Bulletin* 92, 733-742.
- Hemmings-Sykes, S., 2012. MSc Thesis: The influence of faulting on hydrocarbon migration in the Kupe area, south Taranaki Basin, New Zealand. Victoria University of Wellington.
- Higgs, K.E., King, P.R., 2018. Sandstone provenance and sediment dispersal in a complex tectonic setting: Taranaki Basin, New Zealand. *Sedimentary Geology* 372, 112-139.
- Higgs, K.E., King, P.R., Raine, J.I., Sykes, R., Browne, G.H., Crouch, E.M., Baur, J.R., 2012. Sequence stratigraphy and controls on reservoir sandstone distribution in an Eocene marginal marine-coastal plain fairway, Taranaki Basin, New Zealand. *Marine and Petroleum Geology* 32, 110-137.
- Hodgson, D.M., Di Celma, C.N., Brunt, R.L., Flint, S.S., 2011. Submarine slope degradation and aggradation and the stratigraphic evolution of channel–levee systems. *Journal of the Geological Society* 168, 625-628.
- John, C.M., Karner, G.D., Browning, E., Leckie, R.M., Mateo, Z., Carson, B., Lowery, C., 2011. Timing and magnitude of Miocene eustasy derived from the mixed siliciclastic-carbonate stratigraphic record of the northeastern Australian margin. *Earth and Planetary Science Letters* 304, 455-467.
- Kamp, P.J.J., 1999. Tracking crustal processes by FT thermochronology in a forearc high (Hikurangi margin, New Zealand) involving Cretaceous subduction termination and mid-Cenozoic subduction initiation. *Tectonophysics* 307, 313-343.
- Kane, I.A., McCaffrey, W.D., Peakall, J., Kneller, B.C., 2010. Submarine channel levee shape and sediment waves from physical experiments. *Sedimentary Geology* 223, 75-85.
- King, P.R., 2000. Tectonic reconstructions of New Zealand: 40 Ma to the Present. *New Zealand Journal of Geology and Geophysics* 43, 611-638.
- King, P.R., Naish, T.R., Browne, G.H., Field, B.D., Edbrooke, S.W., 2011. Cretaceous to Recent sedimentary patterns in New Zealand. Institute of Geological & Nuclear Sciences.
- King, P.R., Robinson, P.H., 1988. An Overview of Taranaki Region Geology, New Zealand. *Energy Exploration & Exploitation* 6, 213-232.
- King, P.R., Thrasher, G.P., 1992. Post-Eocene Development of the Taranaki Basin, New Zealand: Convergent Overprint of a Passive Margin, *Geology and Geophysics of Continental Margins*. American Association of Petroleum Geologists, p. 0.
- King, P.R., Thrasher, G.P., 1996. Cretaceous Cenozoic geology and petroleum systems of the Taranaki Basin, New Zealand. Institute of Geological & Nuclear Sciences.
- Kneller, B., 2003. The influence of flow parameters on turbidite slope channel architecture. *Marine and Petroleum Geology* 20, 901-910.
- Knox, G.J., 1982. Taranaki Basin, structural style and tectonic setting. *New Zealand Journal of Geology and Geophysics* 25, 125-140.
- Kolla, V., 2007. A review of sinuous channel avulsion patterns in some major deep-sea fans and factors controlling them. *Marine and Petroleum Geology* 24, 450-469.
- Kominz, M.A., Browning, J.V., Miller, K.G., Sugarman, P.J., Mizintseva, S., Scotese, C.R., 2008. Late Cretaceous to Miocene sea-level estimates from the New Jersey and Delaware coastal plain coreholes: an error analysis. *Basin Research* 20, 211-226.

- Kroeger, K.F., Thrasher, G.P., Sarma, M., 2019. The evolution of a Middle Miocene deep-water sedimentary system in northwestern New Zealand (Taranaki Basin): Depositional controls and mechanisms. *Marine and Petroleum Geology* 101, 355-372.
- Kuenen, P.H., 1953. ORIGIN AND CLASSIFICATION OF SUBMARINE CANYONS. *Geological Society of America Bulletin* 64, 1295-1314.
- Leila, M., El-Sheikh, I., Abdelmaksoud, A., Radwan, A.A., 2022. Seismic sequence stratigraphy and depositional evolution of the Cretaceous-Paleogene sedimentary successions in the offshore Taranaki Basin, New Zealand: implications for hydrocarbon exploration. *Marine Geophysical Research* 43, 23.
- Lemay, M., Grimaud, J.-L., Cojan, I., Rivoirard, J., Ors, F., 2020. Geomorphic variability of submarine channelized systems along continental margins: Comparison with fluvial meandering channels. *Marine and Petroleum Geology* 115, 104295.
- Li, Q., Yu, S., Wu, W., Tong, L., Kang, H., 2017. Detection of a deep-water channel in 3D seismic data using the sweetness attribute and seismic geomorphology: a case study from the Taranaki Basin, New Zealand. *New Zealand Journal of Geology and Geophysics* 60, 199-208.
- Lock, R., 1985. The distribution, sedimentology and petroleum prospects of the Moki formation, Taranaki Basin, New Zealand. *Petroleum Report Series PR1150*. Ministry of Economic Development - The government of New Zealand.
- Lubo-Robles, D., Marfurt, K., 2019. Independent component analysis for reservoir geomorphology and unsupervised seismic facies classification in the Taranaki Basin, New Zealand. *Interpretation* 7, SE19-SE42.
- Marfurt, K., 2015. Techniques and best practices in multiattribute display. *Interpretation* 3, B1-B23.
- Mattos, N.H., Alves, T.M., Scully, A., 2019. Structural and depositional controls on Plio-Pleistocene submarine channel geometry (Taranaki Basin, New Zealand). *Basin Research* 31, 136-154.
- Mayall, M., Jones, E., Casey, M., 2006. Turbidite channel reservoirs—Key elements in facies prediction and effective development. *Marine and Petroleum Geology* 23, 821-841.
- Mayall, M., Stewart, I., 2000. The Architecture of Turbidite Slope Channels, in: Weimer, P. (Ed.), *Deep-Water Reservoirs of the World*. GCSSEPM Volume 20. SEPM Society for Sedimentary Geology.
- McHargue, T., Pyrcz, M.J., Sullivan, M.D., Clark, J.D., Fildani, A., Romans, B.W., Covault, J.A., Levy, M., Posamentier, H.W., Drinkwater, N.J., 2011. Architecture of turbidite channel systems on the continental slope: Patterns and predictions. *Marine and Petroleum Geology* 28, 728-743.
- Miller, K.G., Browning, J.V., Schmelz, W.J., Kopp, R.E., Mountain, G.S., Wright, J.D., 2020. Cenozoic sea-level and cryospheric evolution from deep-sea geochemical and continental margin records. *Science Advances* 6, eaaz1346.
- Mortimer, N., 2004. New Zealand's Geological Foundations. *Gondwana Research* 7, 261-272.
- Mouslopoulou, V., Nicol, A., Walsh, J.J., Begg, J.G., Townsend, D.B., Hristopulos, D.T., 2012. Fault-slip accumulation in an active rift over thousands to millions of years and the importance of paleoearthquake sampling. *Journal of Structural Geology* 36, 71-80.
- Niyazi, Y., Eruteya, O.E., Omosanya, K.O., Harishidayat, D., Johansen, S.E., Waldmann, N., 2018. Seismic geomorphology of submarine channel-belt complexes in the Pliocene of the Levant Basin, offshore central Israel. *Marine Geology* 403, 123-138.
- Normark, W.R., 1978. Fan Valleys, Channels, and Depositional Lobes on Modern Submarine Fans: Characters for Recognition of Sandy Turbidite Environments. *AAPG Bulletin* 62, 912-931.

- Omosanya, K.O., 2020. Cenozoic tectonic inversion in the Naglfar Dome, Norwegian North Sea. *Marine and Petroleum Geology* 118, 104461.
- Palmer, J.A., Andrews, P.B., 1993. Cretaceous–Tertiary sedimentation and implied tectonic controls on the structural evolution of Taranaki Basin, New Zealand. *South Pacific sedimentary basins. Sedimentary basins of the world* 2, 309-328.
- Peakall, J., Sumner, E.J., 2015. Submarine channel flow processes and deposits: A process-product perspective. *Geomorphology* 244, 95-120.
- Pettingill, H., 2004. 2. Global Overview of Deepwater Exploration and Production, in: Weimer, P. (Ed.), *Petroleum Systems of Deepwater Settings*. Society of Exploration Geophysicists, pp. 2-1-2-40.
- Pickering, K., Hiscott, R., 2015. *Deep Marine Systems: Processes, Deposits, Environments, Tectonic and Sedimentation*. John Wiley & Sons.
- Pickering, K.T., Corregidor, J., Clark, J.D., 2015. Architecture and stacking patterns of lower-slope and proximal basin-floor channelised submarine fans, Middle Eocene Ainsa System, Spanish Pyrenees: An integrated outcrop–subsurface study. *Earth-Science Reviews* 144, 47-81.
- Pigott, J.D., Kang, M.-H., Han, H.-C., 2013. First order seismic attributes for clastic seismic facies interpretation: Examples from the East China Sea. *Journal of Asian Earth Sciences* 66, 34-54.
- Posamentier, H.W., 2003. Depositional elements associated with a basin floor channel-levee system: case study from the Gulf of Mexico. *Marine and Petroleum Geology* 20, 677-690.
- Posamentier, H.W., Kolla, V., 2003. Seismic Geomorphology and Stratigraphy of Depositional Elements in Deep-Water Settings. *Journal of Sedimentary Research* 73, 367-388.
- Reilly, C., Nicol, A., Walsh, J.J., Seebeck, H., 2015. Evolution of faulting and plate boundary deformation in the Southern Taranaki Basin, New Zealand. *Tectonophysics* 651-652, 1-18.
- Rider, M.H., 1986. *The geological interpretation of well logs*. John Wiley and Sons, Inc, United States.
- Roncaglia, L., Fohrmann, M., Milner, M., Morgans, H.E.G., Crundwell, M.P., 2013. Well log stratigraphy in the central and southern offshore area of the taranaki basin, New Zealand. GNS Science Report.
- Sahoo, T.R., Nicol, A., Browne, G.H., Strogon, D.P., 2020. Evolution of a Normal Fault System Along Eastern Gondwana, New Zealand. *Tectonics* 39, e2020TC006181.
- Sena, A., Castillo, G., Chesser, K., Voisey, S., Estrada, J., Carcuz, J., Carmona, E., Hodgkins, P., 2011. Seismic reservoir characterization in resource shale plays: Stress analysis and sweet spot discrimination. *The Leading Edge* 30, 758-764.
- Shepard, F.P., 1981. Submarine canyons: multiple causes and long-time persistence. *AAPG Bulletin* 65, 1062-1077.
- Silver, C., Bedle, H., 2021. Evolution of a Late Miocene Deep-Water Depositional System in the Southern Taranaki Basin, New Zealand. *Geosciences* 11, 329.
- Stagpoole, V., Nicol, A., 2008. Regional structure and kinematic history of a large subduction back thrust: Taranaki Fault, New Zealand. *Journal of Geophysical Research: Solid Earth* 113.
- Stow, D.A.V., Mayall, M., 2000. Deep-water sedimentary systems: New models for the 21st century. *Marine and Petroleum Geology* 17, 125-135.
- Straub, K.M., Mohrig, D., Pirmez, C., 2012. Architecture of an Aggradational Tributary Submarine-Channel Network on the Continental Slope Offshore Brunei Darussalam, in: Prather, B.E., Deptuck, M.E., Mohrig, D., Hoorn, B.V., Wynn, R.B. (Eds.), *Application of the Principles of Seismic*

Geomorphology to Continental Slope and Base-of-Slope Systems: Case Studies from SeaFloor and Near-Sea Floor Analogues. SEPM Society for Sedimentary Geology, p. 0.

Strogen, D.P., 2011. Updated paleogeographic maps for the Taranaki Basin and surrounds. Lower Hutt, New Zealand: GNS Science.

Strogen, D.P., Bland, K.J., Nicol, A., King, P.R., 2014. Paleogeography of the Taranaki Basin region during the latest Eocene–Early Miocene and implications for the ‘total drowning’ of Zealandia. *New Zealand Journal of Geology and Geophysics* 57, 110-127.

Strogen, D.P., Seebeck, H., Nicol, A., King, P.R., 2017. Two-phase Cretaceous–Paleocene rifting in the Taranaki Basin region, New Zealand; implications for Gondwana break-up. *Journal of the Geological Society* 174, 929-946.

Sutherland, R., Dickens, G.R., Blum, P., Agnini, C., Alegret, L., Asatryan, G., Bhattacharya, J., Bordenave, A., Chang, L., Collot, J., Cramwinckel, M.J., Dallanave, E., Drake, M.K., Etienne, S.J.G., Giorgioni, M., Gurnis, M., Harper, D.T., Huang, H.-H.M., Keller, A.L., Lam, A.R., Li, H., Matsui, H., Morgans, H.E.G., Newsam, C., Park, Y.-H., Pascher, K.M., Pekar, S.F., Penman, D.E., Saito, S., Stratford, W.R., Westerhold, T., Zhou, X., 2020. Continental-scale geographic change across Zealandia during Paleogene subduction initiation. *Geology* 48, 419-424.

Uruski, C., 2015. The contribution of offshore seismic data to understanding the evolution of the New Zealand continent. Geological Society, London, Special Publications 413, 35-51.

Uruski, C.I., 2010. New Zealand’s deepwater frontier. *Marine and Petroleum Geology* 27, 2005-2026.

Voggenreiter, W.R., 1993. Structure and evolution of the Kapuni Anticline, Taranaki Basin, New Zealand: evidence from the Kapuni 3D seismic survey. *New Zealand journal of geology and geophysics* 36, 77-94.

Weimer, P., Pettingill, H., 2020. The History of Deepwater Exploration, Part 2, AAPG Explorer. AAPG.

Wunderlich, A., Kobstaedt, A., 2017. Reservoir characterization of the miocene moki formation in the maari/manaua field area, southern taranaki basin, new zealand: Integration of depositional and diagenetic concepts., *New Zealand Petroleum Conference*.

Zachos, J.C., Dickens, G.R., Zeebe, R.E., 2008. An early Cenozoic perspective on greenhouse warming and carbon-cycle dynamics. *Nature* 451, 279.

Zeng, H., 2010. Stratal slicing: Benefits and challenges. *The Leading Edge* 29, 1040-1047.

Zhang, G., Qu, H., Chen, G., Zhao, C., Zhang, F., Yang, H., Zhao, Z., Ma, M., 2019. Giant discoveries of oil and gas fields in global deepwaters in the past 40 years and the prospect of exploration. *Journal of Natural Gas Geoscience* 4, 1-28.

## **Geomorphologic Controls on the Evolution of Submarine Channels in the Clifdenian-Tongaporutuan Interval of the Southern Taranaki Basin, offshore New Zealand.**

Dicky Harishidayat<sup>1\*</sup>, Chris Larsen<sup>2‡</sup>, Kamaldeen. O.L. Omosanya<sup>2</sup>

<sup>1</sup>Department of Geosciences, College of Petroleum Engineering and Geosciences, King Fahd University of Petroleum and Minerals, Dhahran.

<sup>2</sup>Department of Geoscience and Petroleum, Norwegian University of Science and Technology, Trondheim.

\*Corresponding author: Dicky Harishidayat ([dicky.hidayat@kfupm.edu.sa](mailto:dicky.hidayat@kfupm.edu.sa) or [dickyharishidayat@gmail.com](mailto:dickyharishidayat@gmail.com)).

‡Now Data Analyst at TINE Norway.

### **Figures**

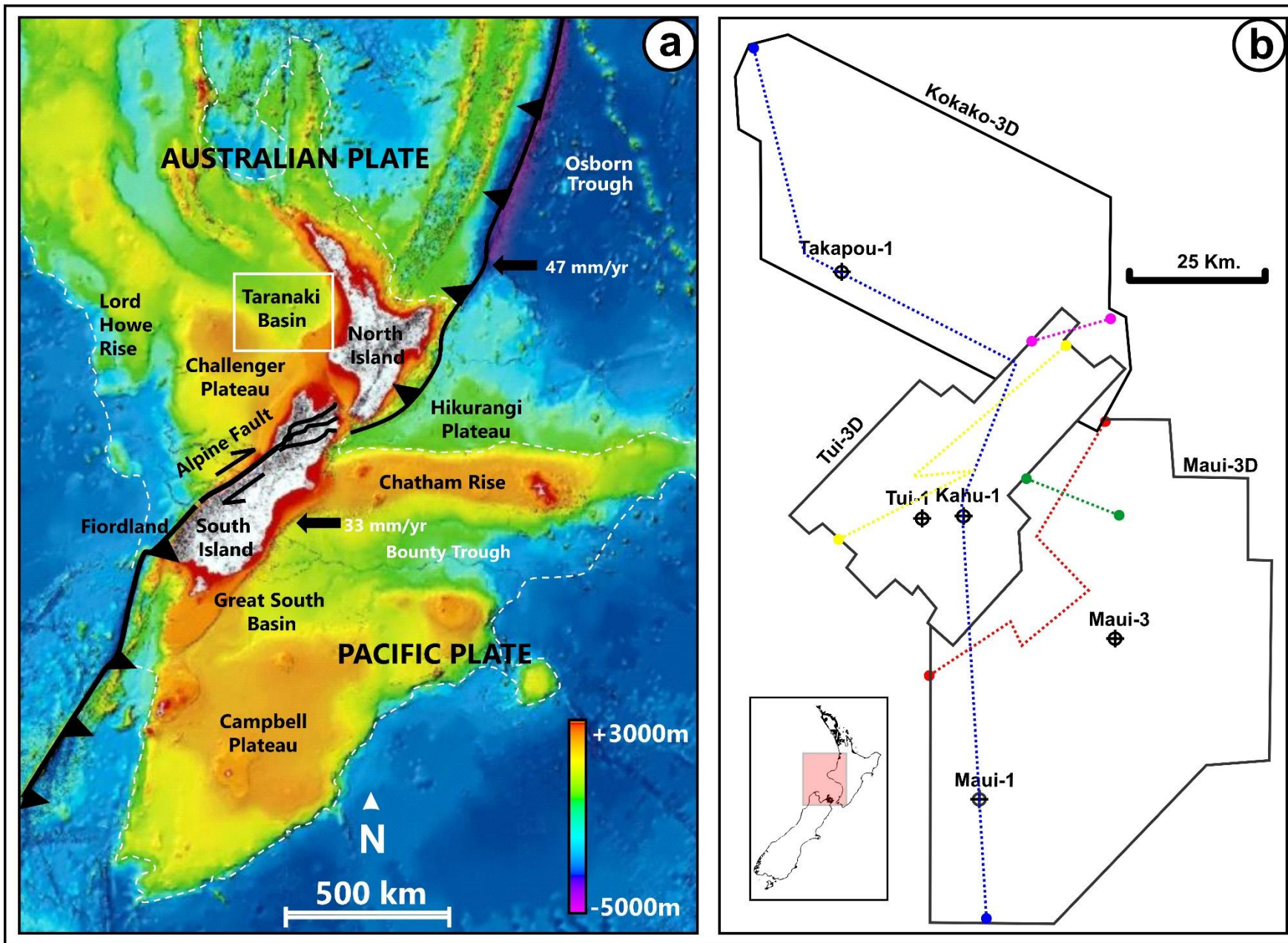


**Figure 1.** A 250 m gridded bathymetric-topographic map showing the structural elements of New Zealand and location of the study area in white rectangle. The bathymetry map was downloaded from [www.niwa.co.nz](http://www.niwa.co.nz). b) Map showing the location and outline of the three seismic surveys and wellbore used in this study. Color lines are seismic section location on the Figures 7 (Red), 4 (Blue), 5 (Pink), 5 (Green), and 6 (yellow).

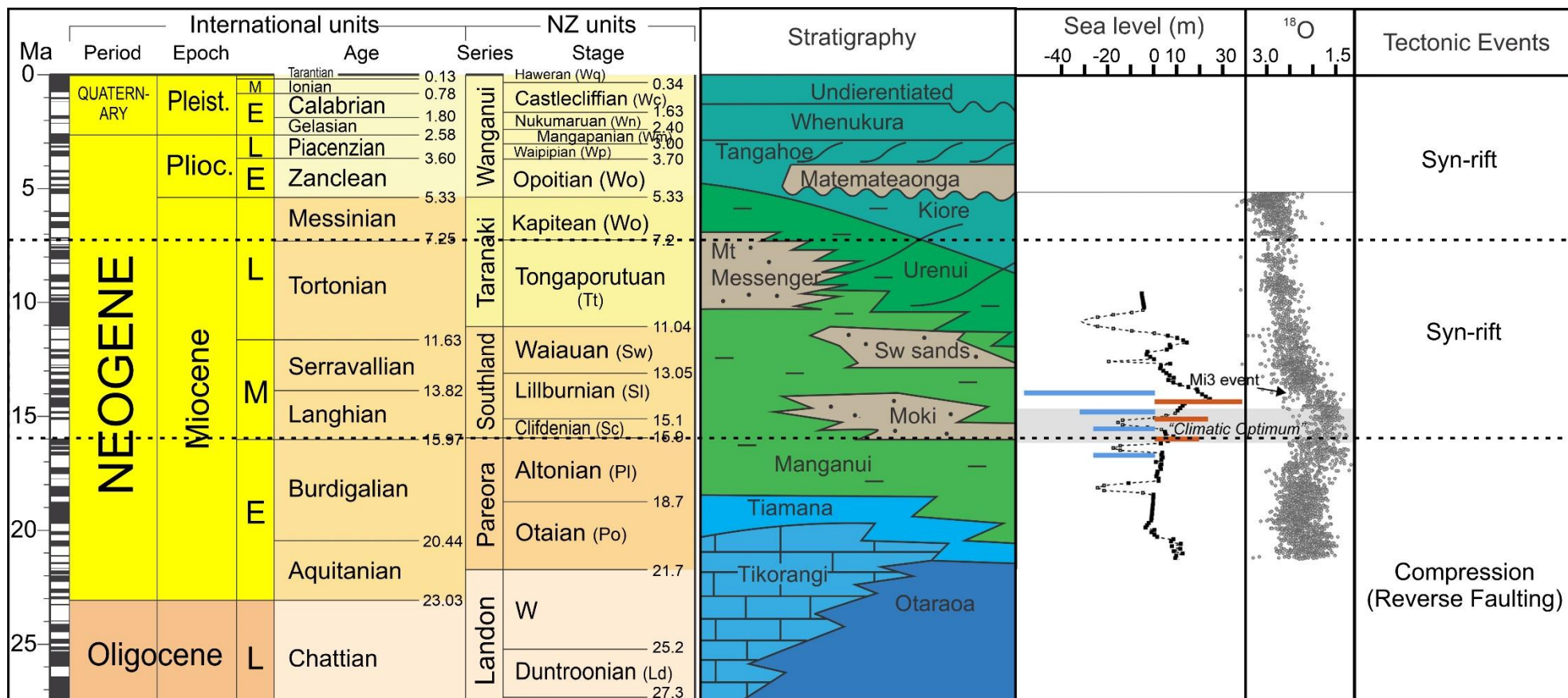


**Figure 2.** Cenozoic lithostratigraphy of the study area (dotted line) showing ages of the formations (Roncaglia et al. 2013), global sea-level curve (Kominz et al. 2008; Kroeger et al. 2019) with sea level falls (blue bars) and rises (orange bars) of John et al., (2011), global oxygen isotopes (Kroeger et al. 2019; Miller et al. 2020; Zachos et al. 2008) and the principal tectonic events during their deposition (King and Thrasher, 1992).

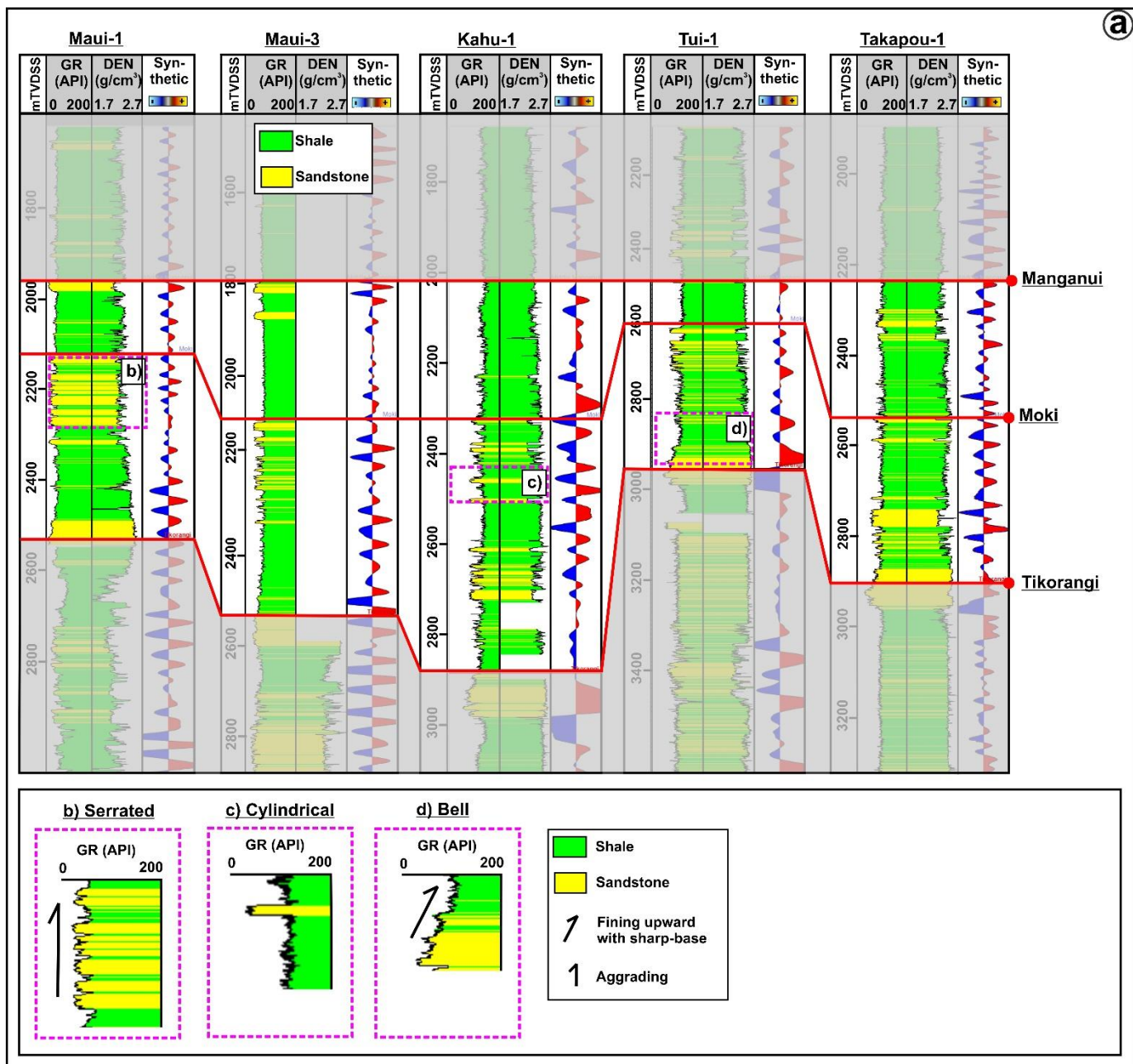


**Figure 3.** a) Stratigraphic correlation panel between wellbores Maui-1, Maui-3, Kahu-1, Tui-1 and Takapou-1 showing the interpreted lithology, synthetic seismogram and Formation name in this study. b) Gamma-ray stacking pattern of representative types that indicated submarine channel. The locations of the wells is shown in Figure 1b.

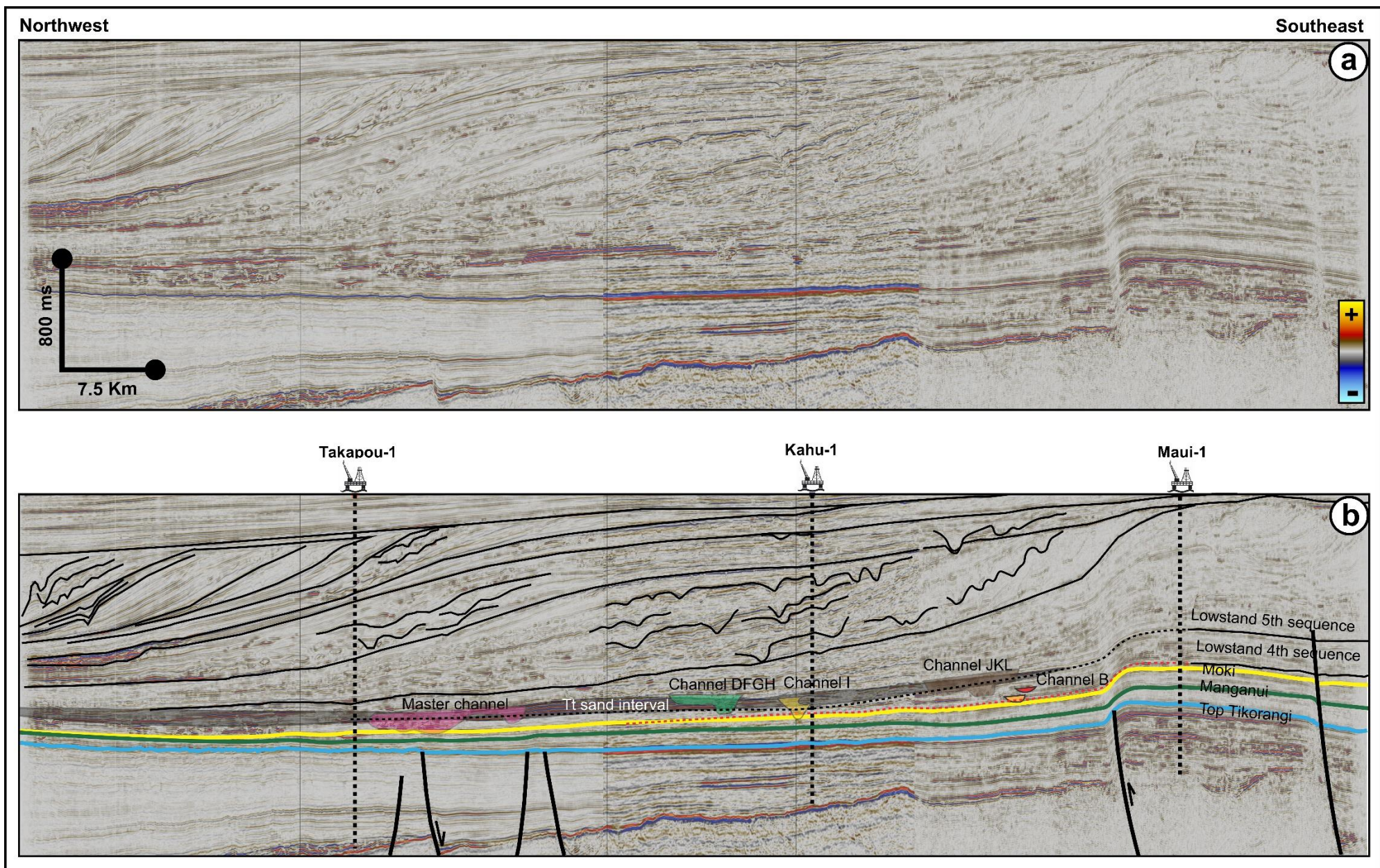


**Figure 4.** NW-SE arbitrary line showing the overall seismic stratigraphic of the study area. The seismic line passes through wellbore Tokapou-1, Kahu-1 and Maui-1. The interval of interest in this work is the Clifdenian-Tongaporutuan where several submarine channels of Middle Miocene age are buried. See the blue profile on Figure 1b for section location.

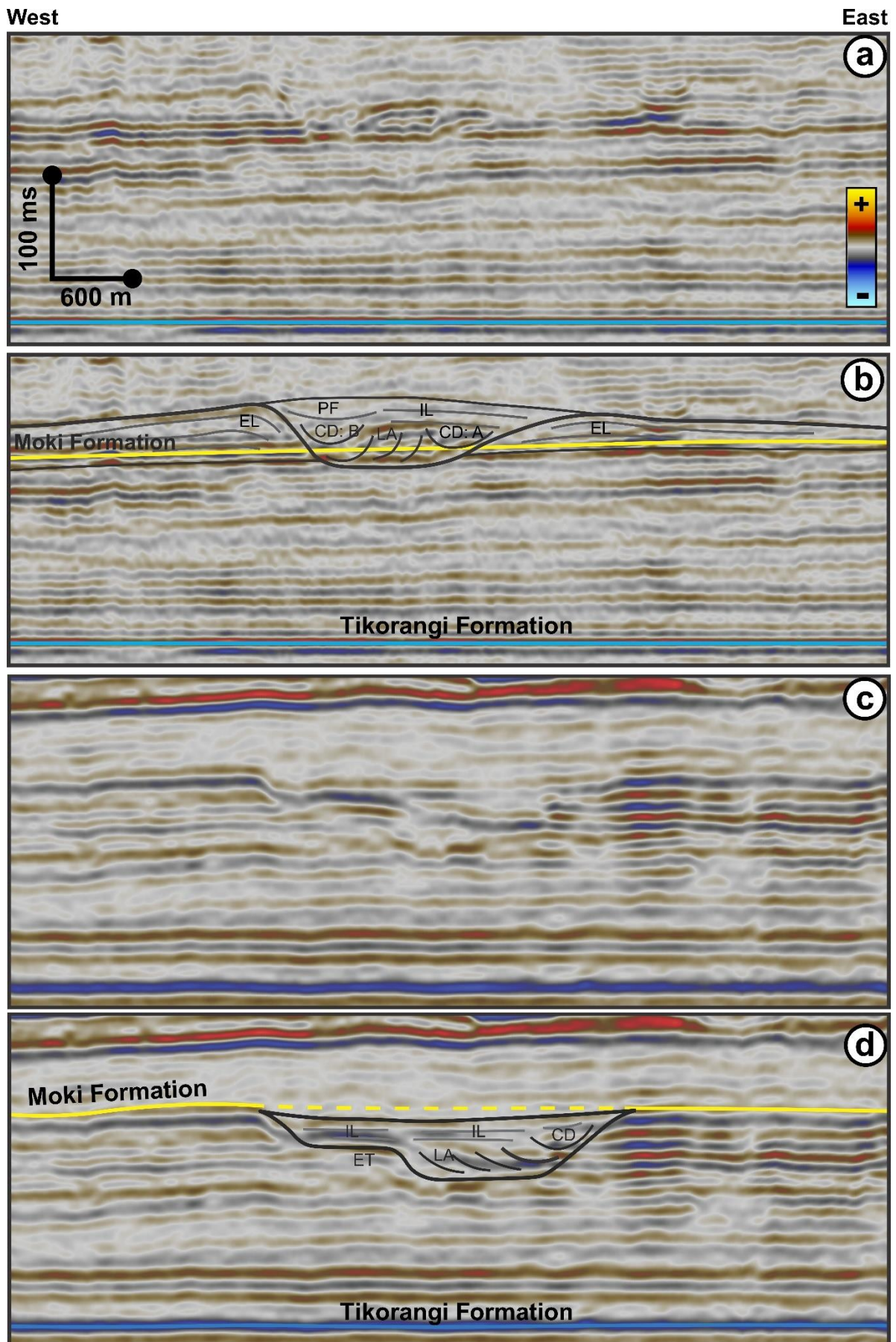


**Figure 5.** (A and B) Uninterpreted and interpreted W-E seismic section through the pink profile showing the elements and architectural outlook of seismic expression of channel A in the northern part of the study area. Note that the seismic profile is flattened at the top Tikorangi Formation level. CD:A/B = channel deposits for channels A and B. (C and D) Uninterpreted and interpreted W-E seismic section through the green profile showing the elements and architectural outlook of seismic expression of channel A in the central part of the study area. Note that the seismic section is flattened at the top Tikorangi Formation level. CD = channel deposits; ET = erosional terrace; LA = lateral accretion packages; EF = external levees; PF = passive fill and IL = internal levees. See location of seismic profile in Figure 1b.

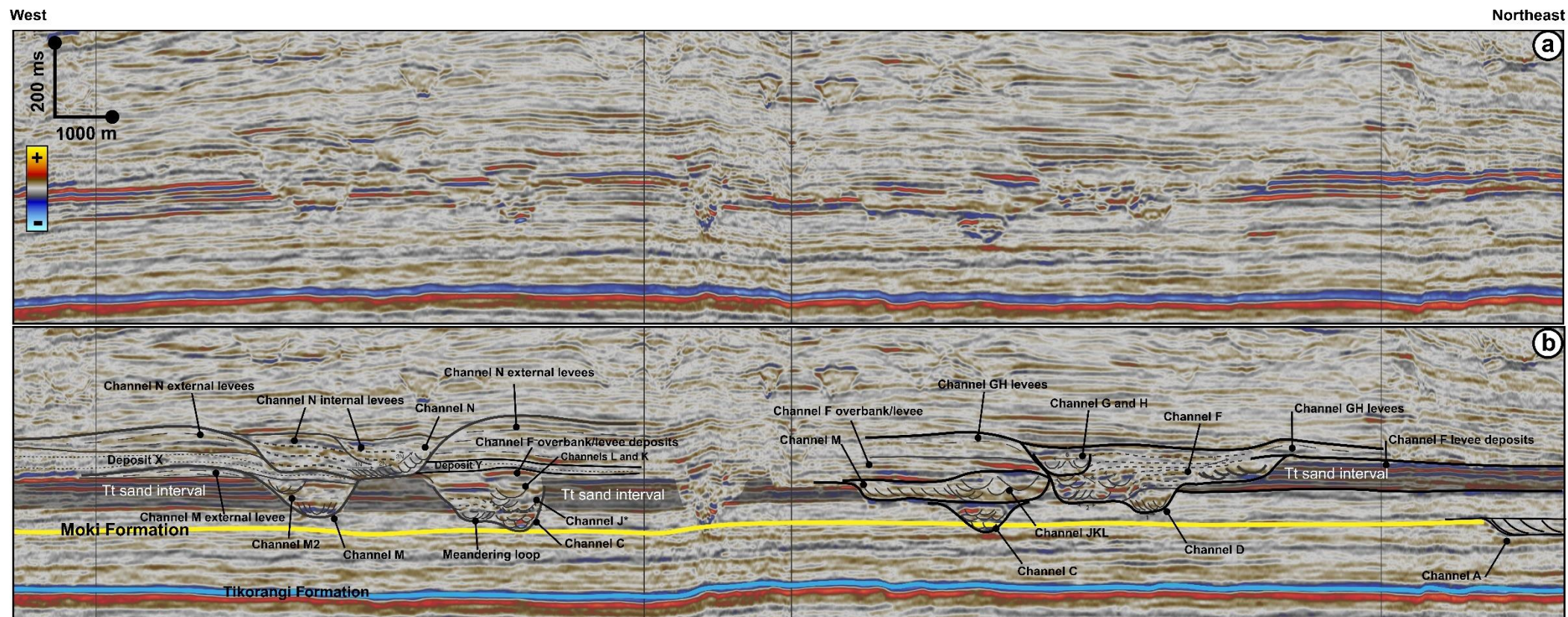


**Figure 6.** (A) and (B) Uninterpreted and interpreted W-E seismic section through the yellow profile showing the seismic expression of channel C, JKL, G, H, and D. Note that the seismic profile is flattened at the top Moki Formation level (C) and (D) Uninterpreted and interpreted W-E seismic section through transect IIIa showing the seismic expression of channel M, C, J and N. See location of seismic in Figure 1b.

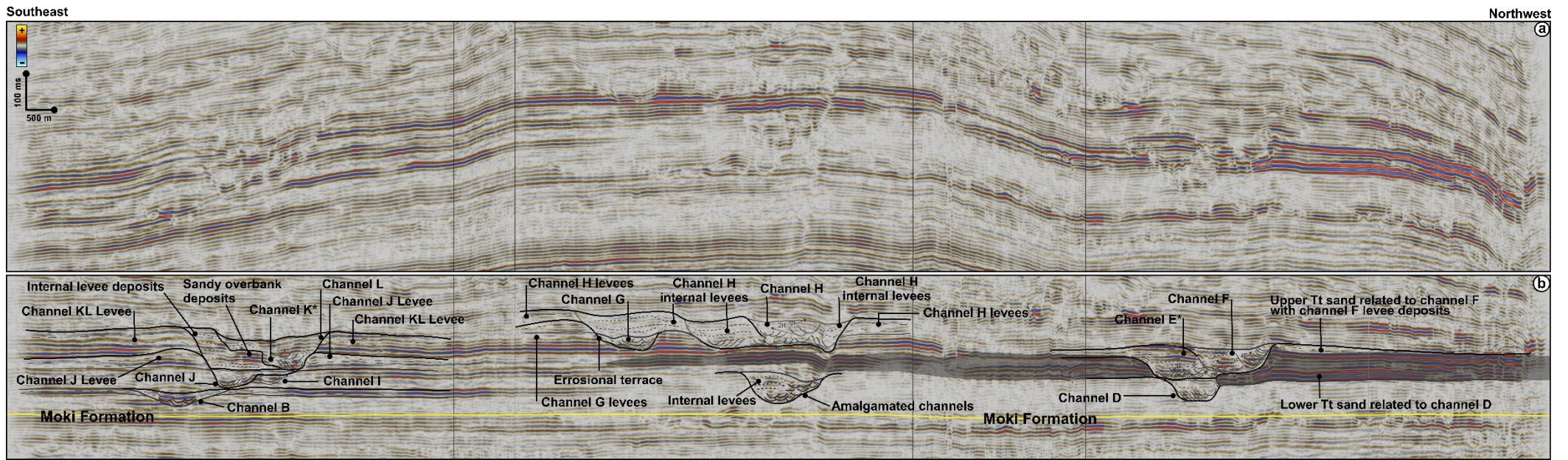


**Figure 7.** Uninterpreted and interpreted SE-NW seismic section through the red profile showing the seismic expression of (A) channels B, J, I, K and L (B) channel E, F and D See location of seismic in Figure 1b.

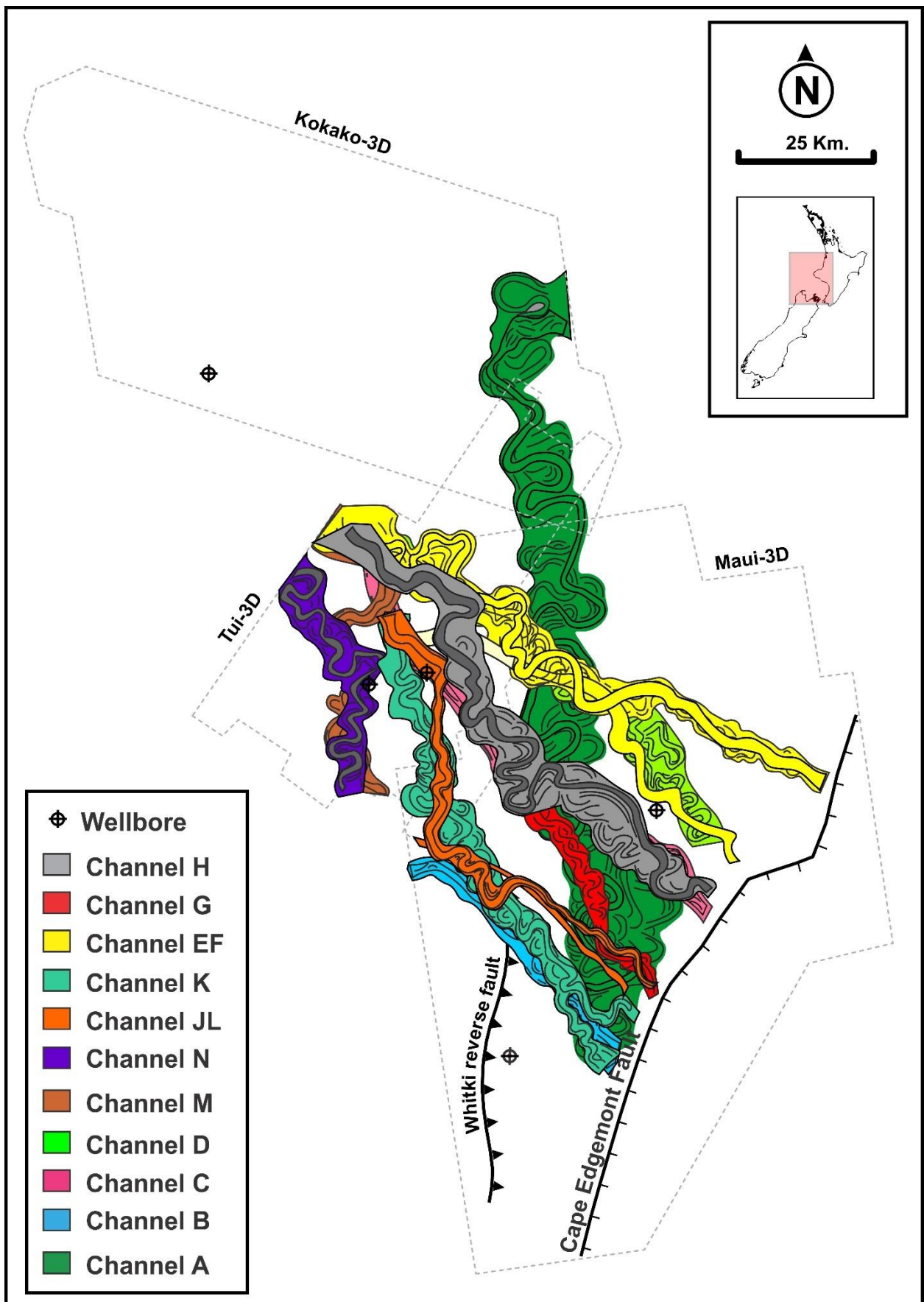


**Figure 8.** Schematic map showing the lateral and spatial interactions between the interpreted channels in the study area. Most of the channels are terminated on the hanging wall section of the Cape Edgemont Fault.

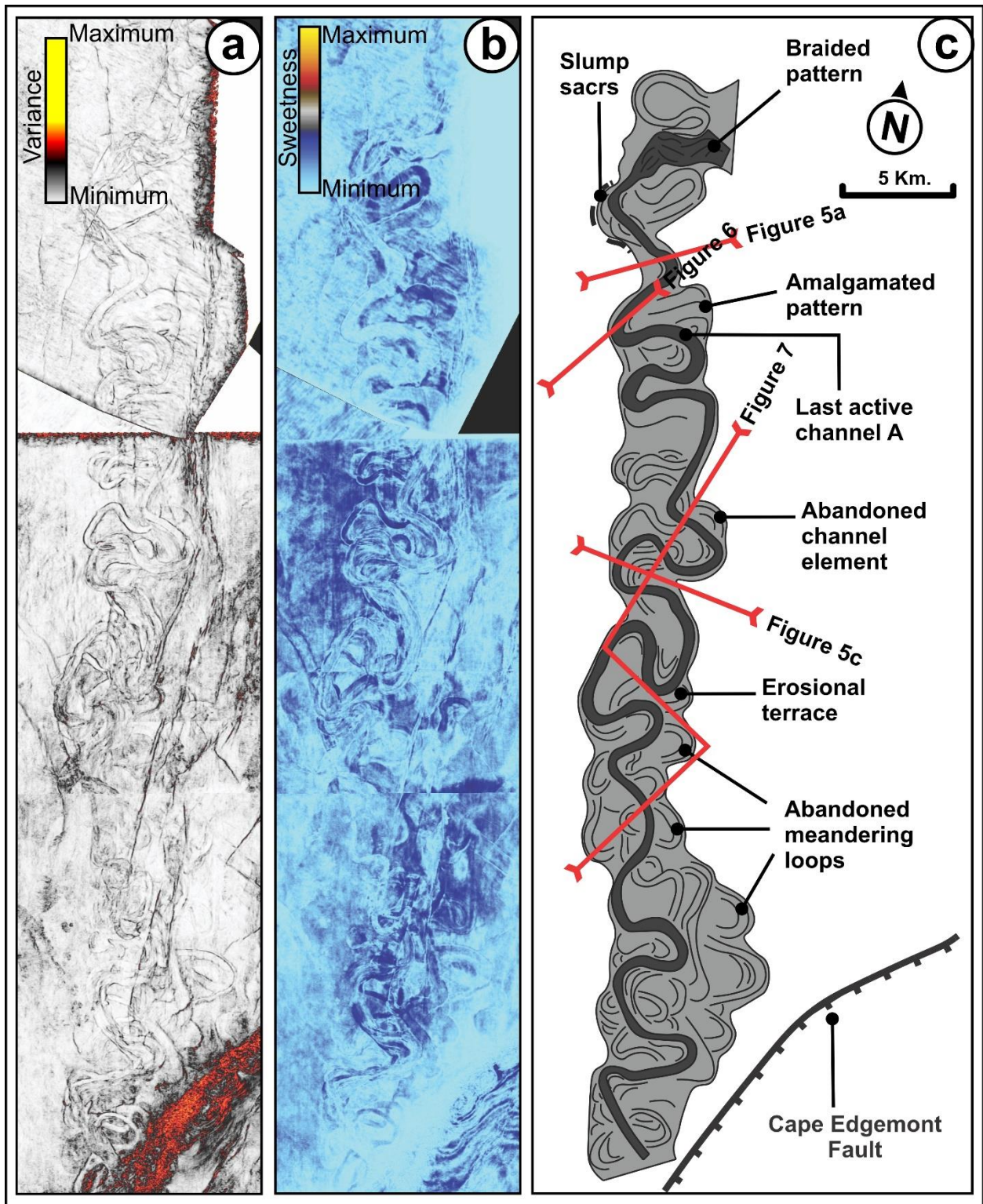


**Figure 9.** (a) to (c) Variance time slice, sweetness time slice and the schematic diagram showing the seismic expression of channel A. Note that dark blue color on the sweetness map within the channel belt may indicate the presence of sand-prone deposits.

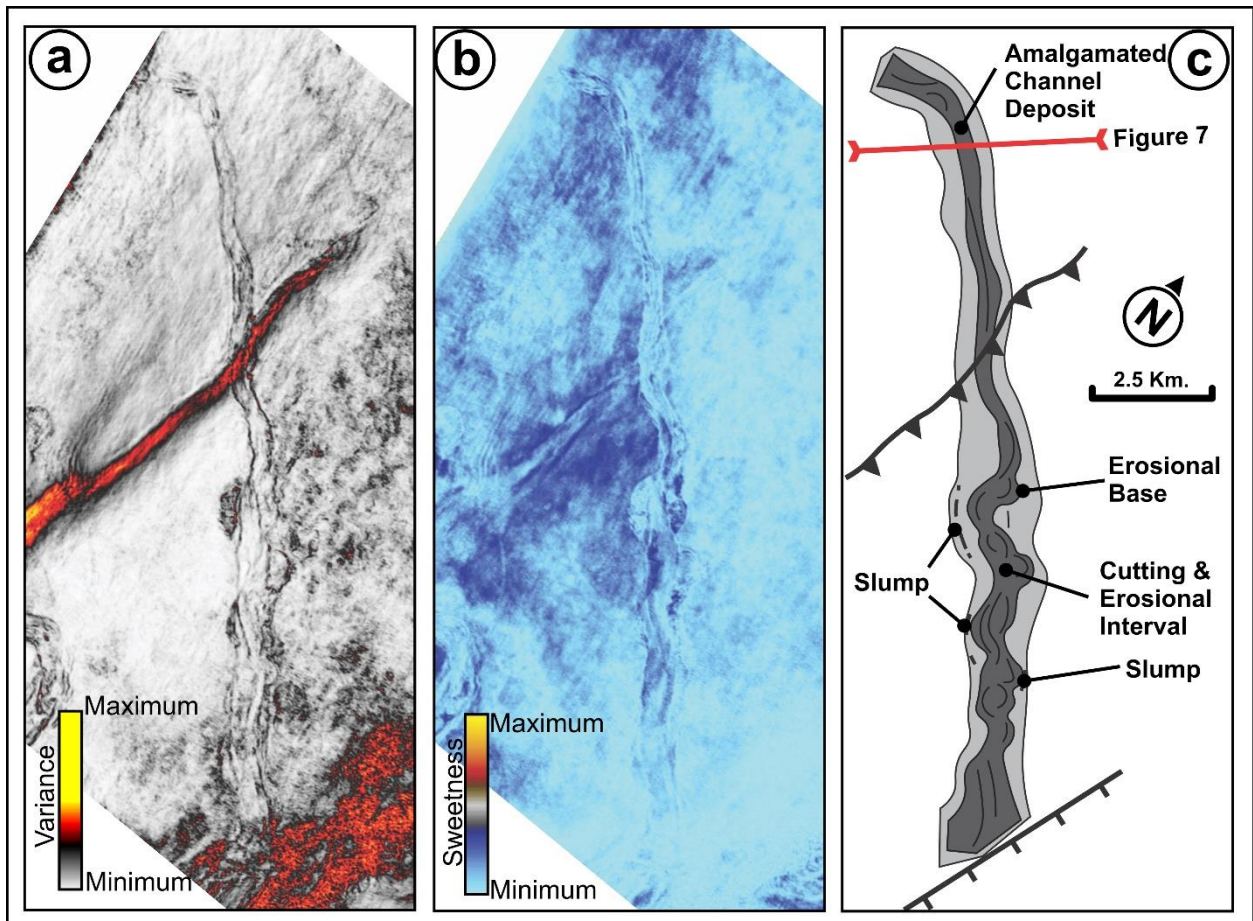


**Figure 10.** (a) to (c) Variance time map, sweetness map and the schematic diagram showing the seismic expression of channel B. Note that dark blue color on the sweetness map within the channel belt may indicate the presence of sand-prone deposits.

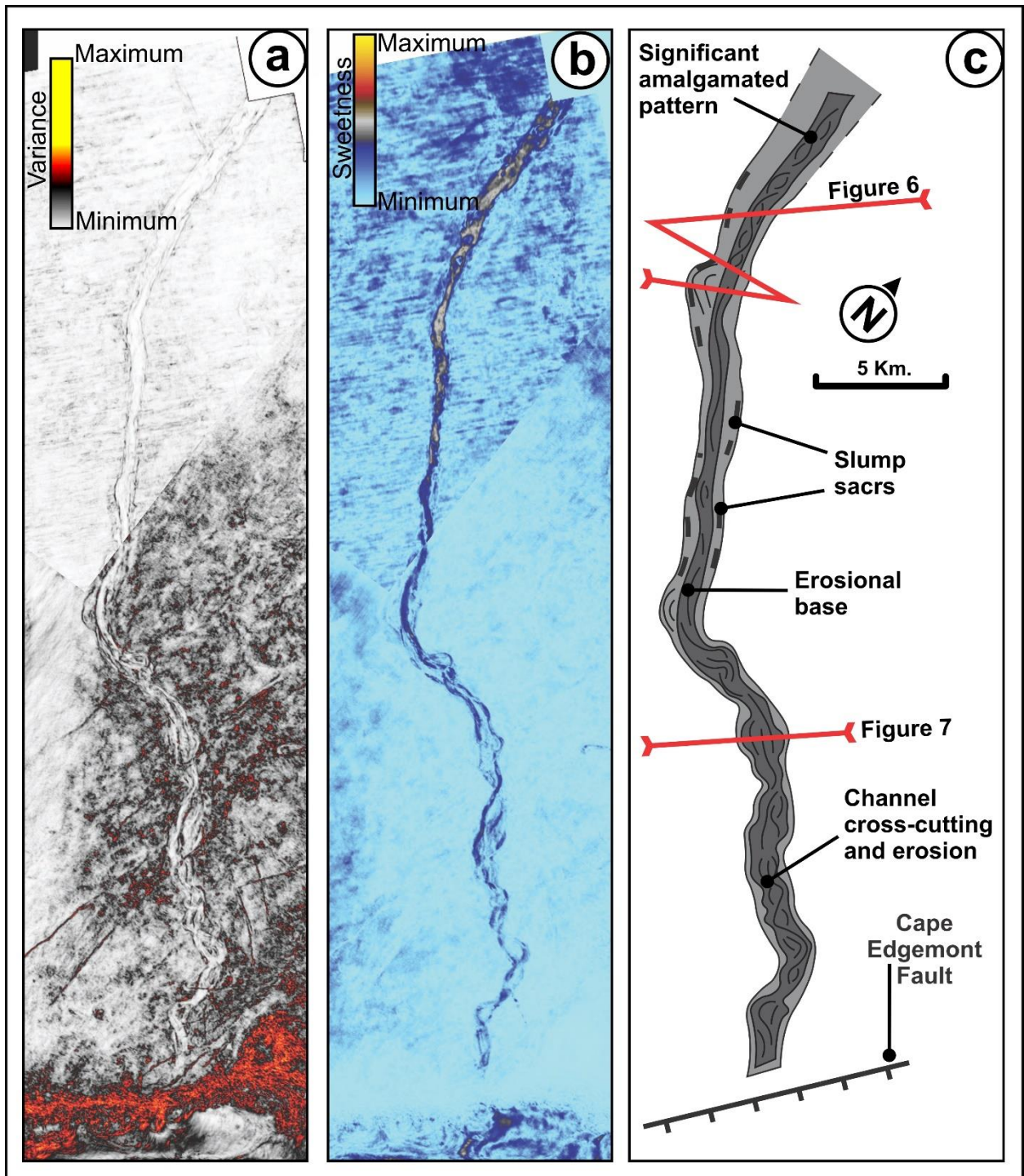


**Figure 11.** (a) to (c) Variance time map, sweetness map and the schematic diagram showing the seismic expression of channel C. Note that dark blue color on the sweetness map within the channel belt may indicate the presence of sand-prone deposits.

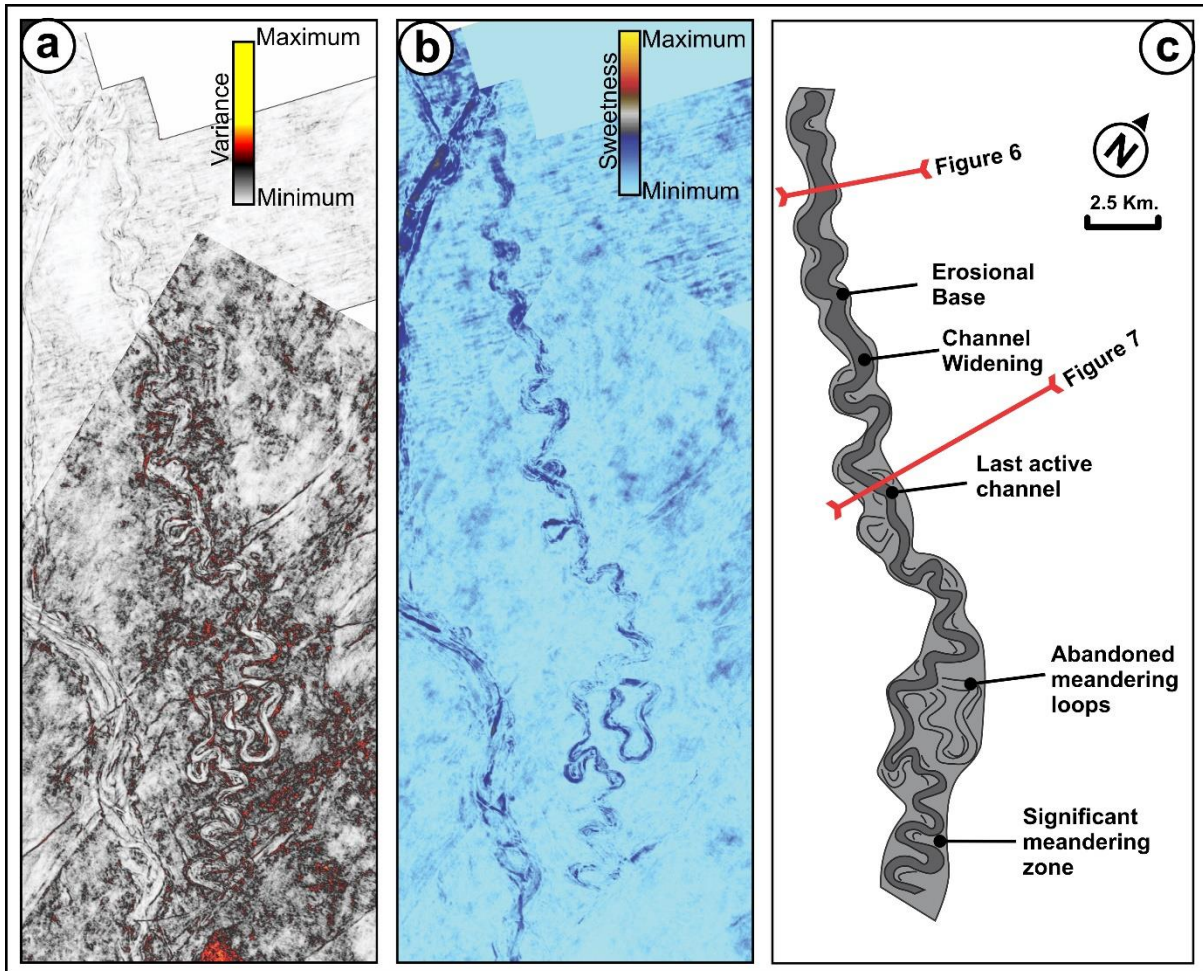


**Figure 12.** (a) to (c) Variance time map, sweetness map and the schematic diagram showing the seismic expression of channel D. Note that dark blue color on the sweetness map within the channel belt may indicate the presence of sand-prone deposits.

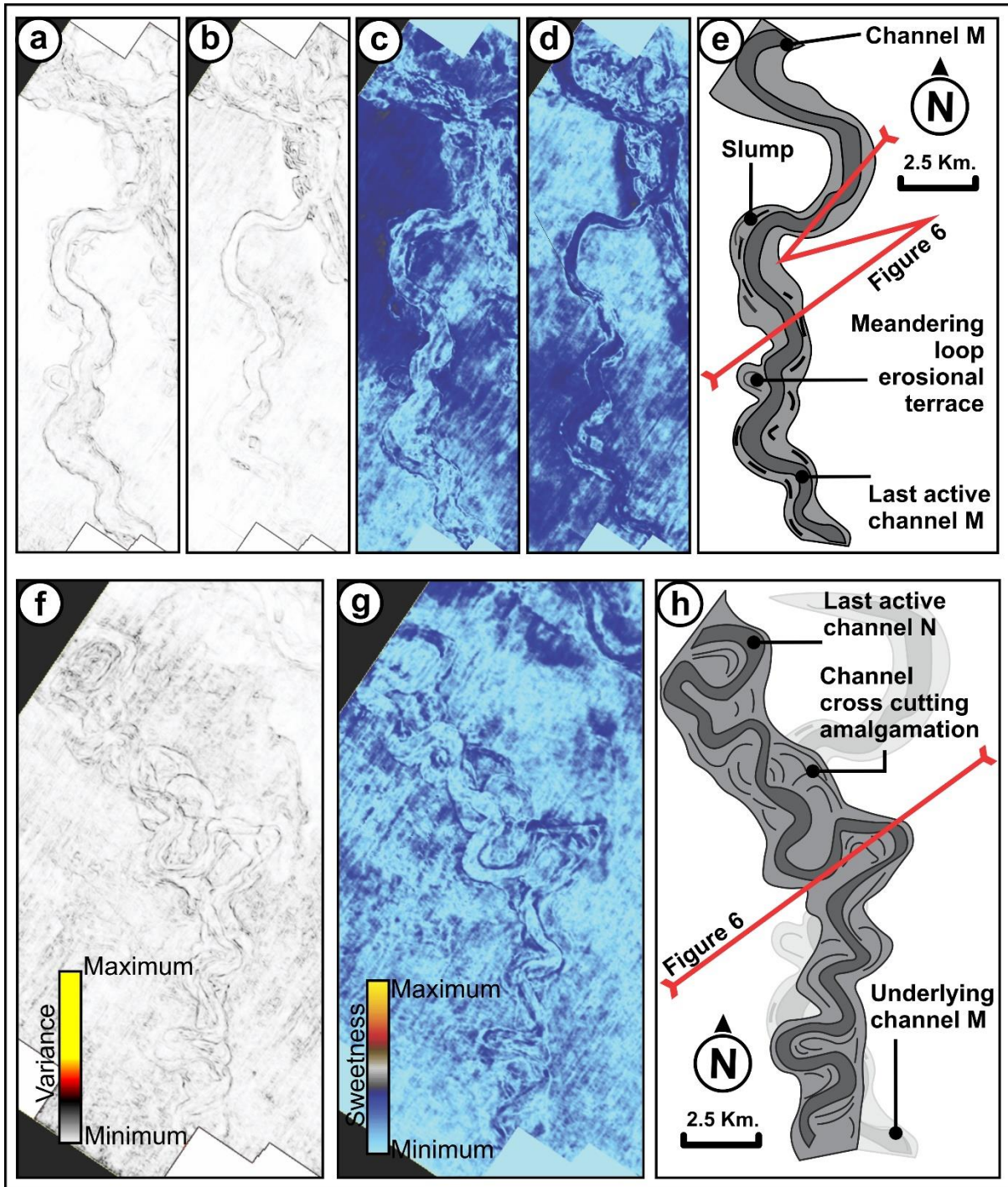


**Figure 13.** (a) to (c) Variance time map, sweetness map and the schematic diagram showing the seismic expression of channels MN. Note that dark blue color on the sweetness map within the channel belt may indicate the presence of sand-prone deposits.

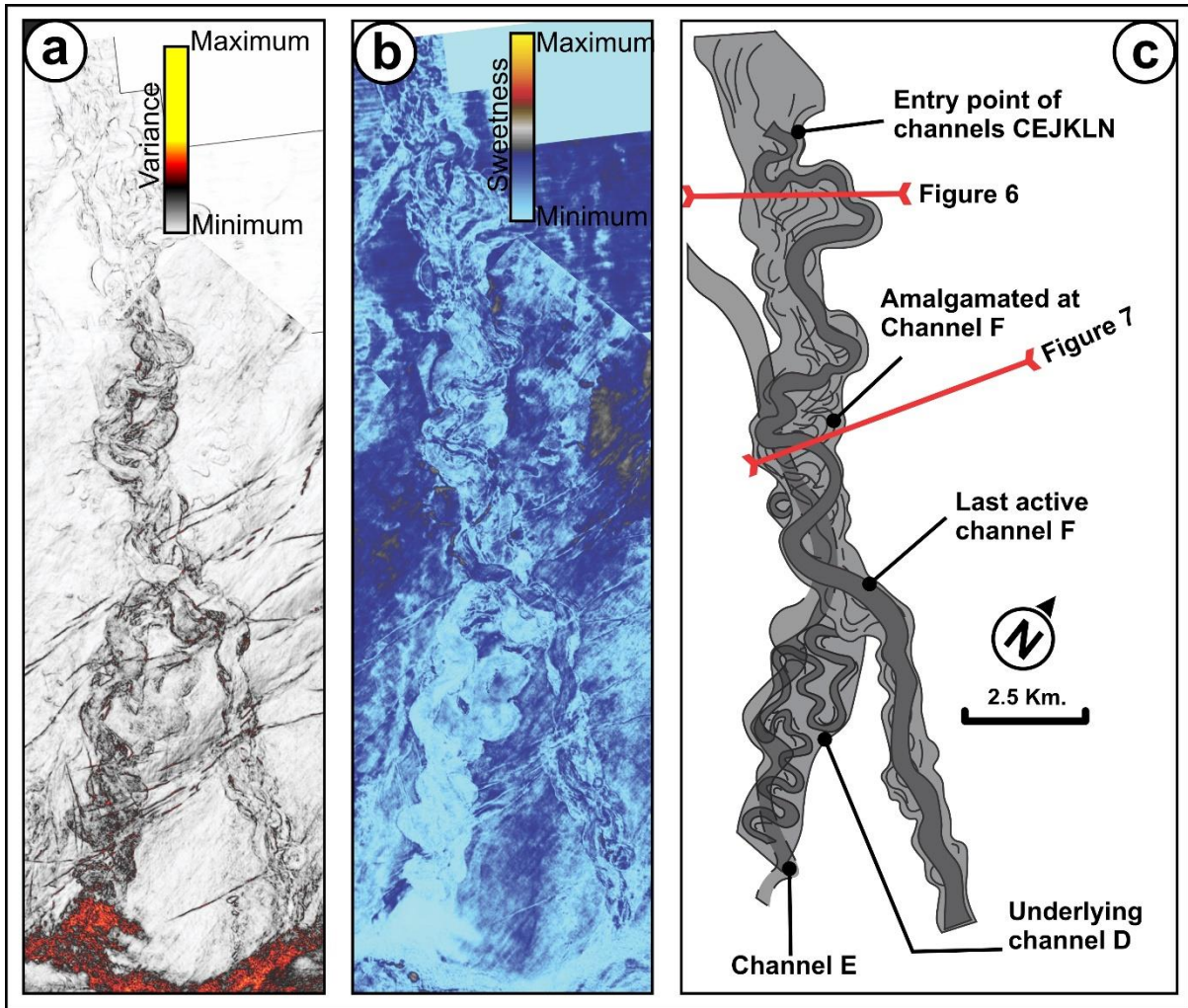


**Figure 14.** (a) to (c) Variance time map, sweetness map and the schematic diagram showing the seismic expression of channels EF and KL. Note that dark blue color on the sweetness map within the channel belt may indicate the presence of sand-prone deposits.

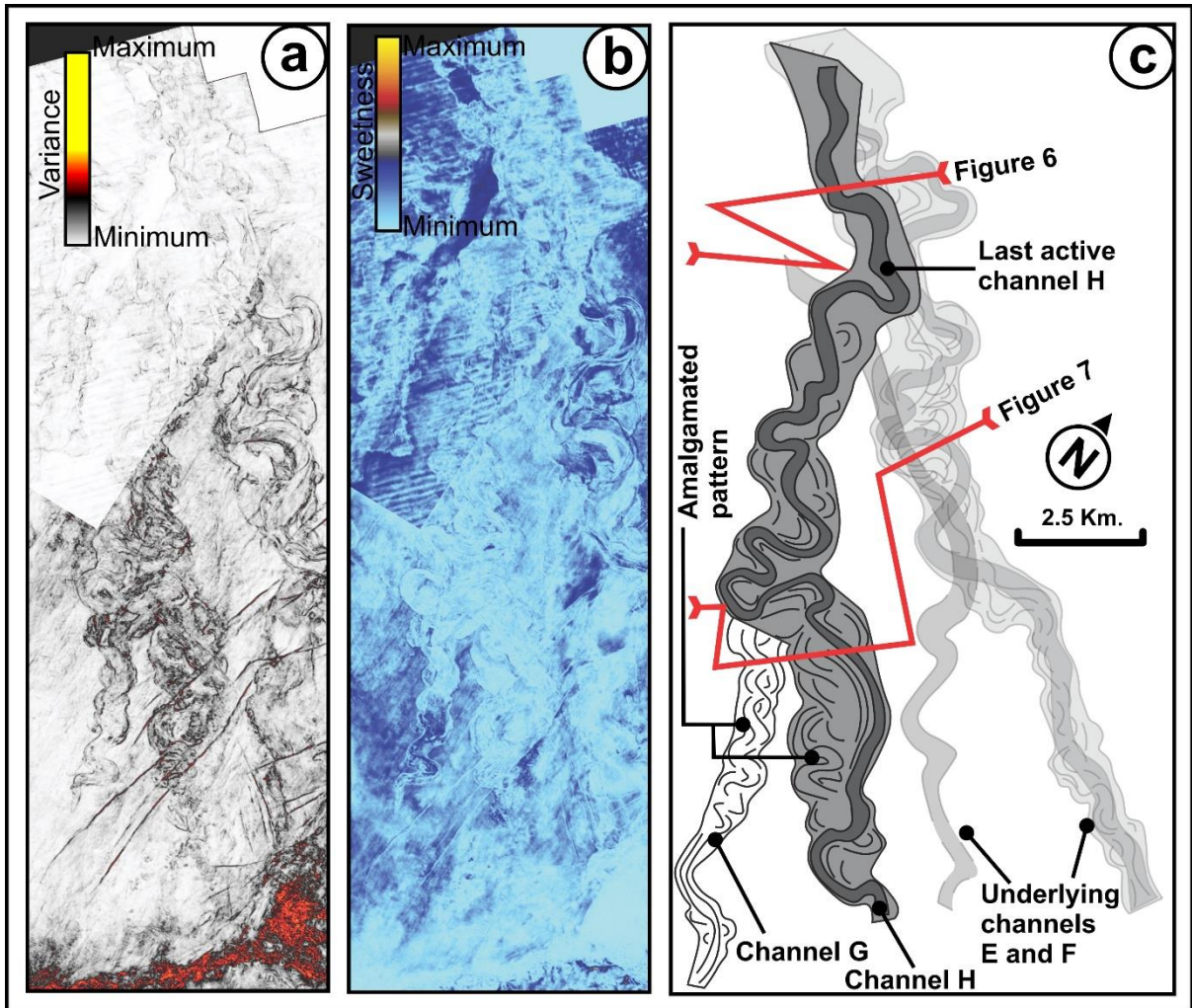


**Figure 15.** (a) to (c) Variance time map, sweetness map and the schematic diagram showing the seismic expression of channels GH. Note that dark blue color on the sweetness map within the channel belt may indicate the presence of sand-prone deposits.

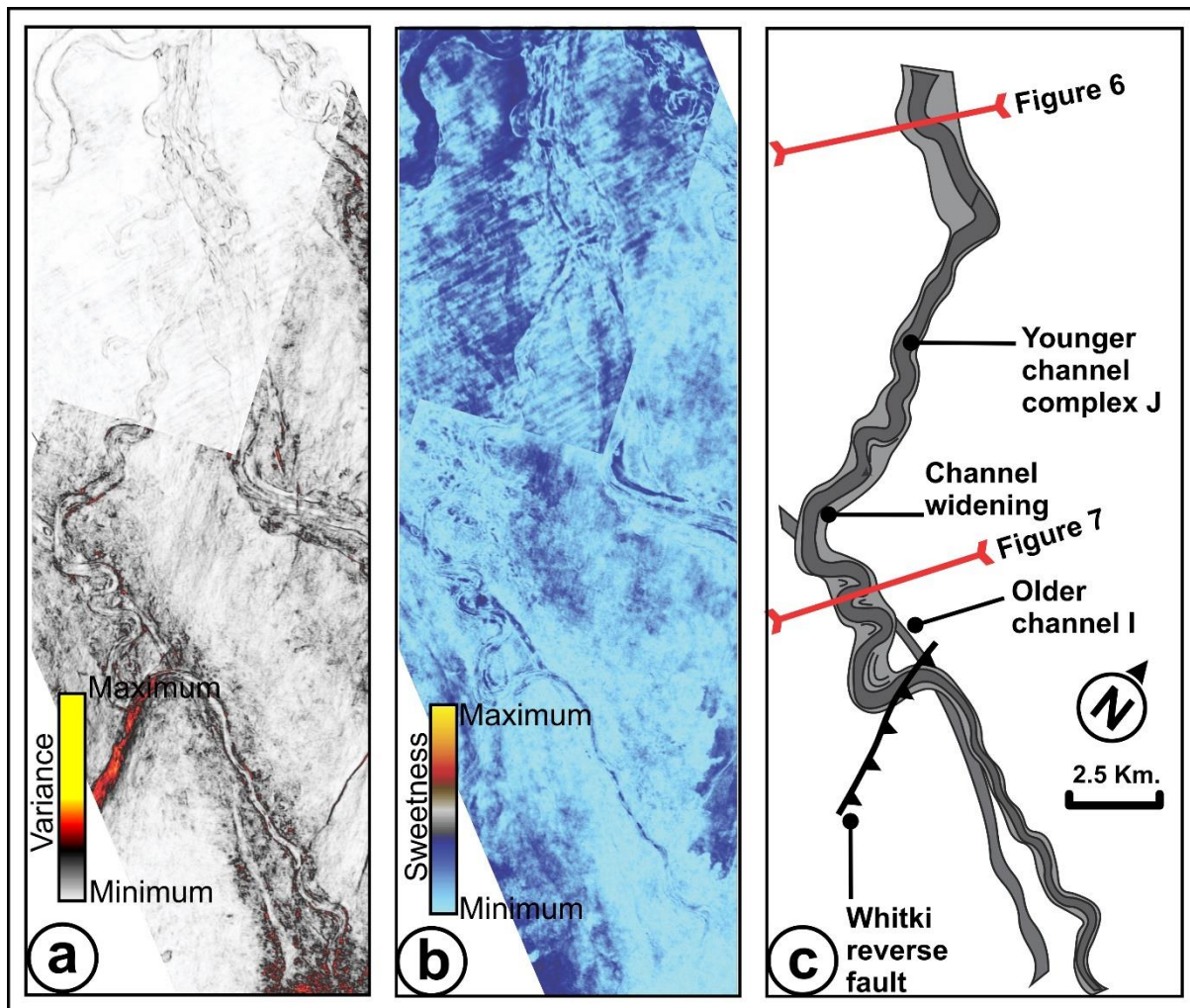


**Figure 16.** (a) to (c) Variance time map, sweetness map and the schematic diagram showing the seismic expression of channels IJ. Note that dark blue color on the sweetness map within the channel belt may indicate the presence of sand-prone deposits.

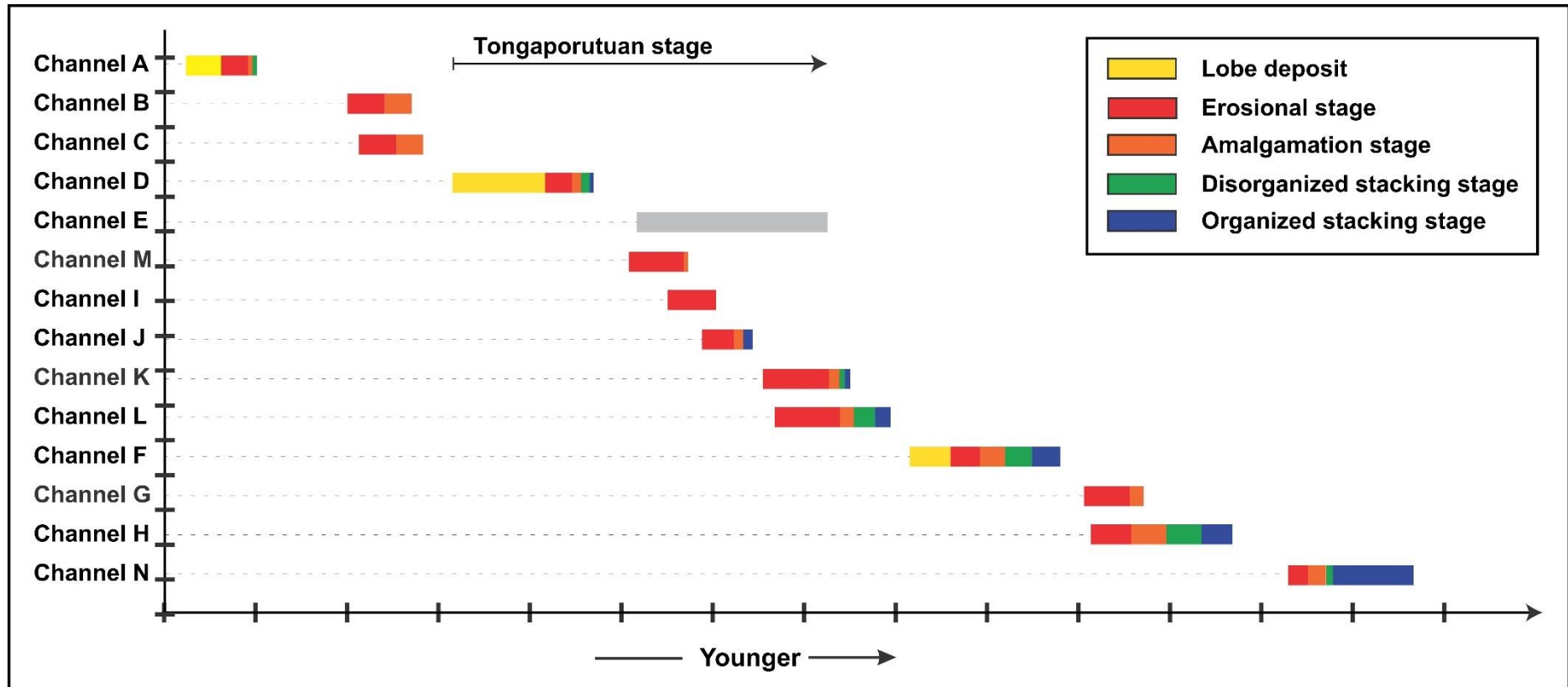


**Figure 17.** Timeline showing the temporal evolution of the interpreted submarine channel. The black arrow is the approximate time of a lowstand system tract based on the interpretations of Kroeger et al. (2019), placing this as early Tongaporutuan. The gray bar for channel E is the uncertainty related to its relative age and depositional architecture.

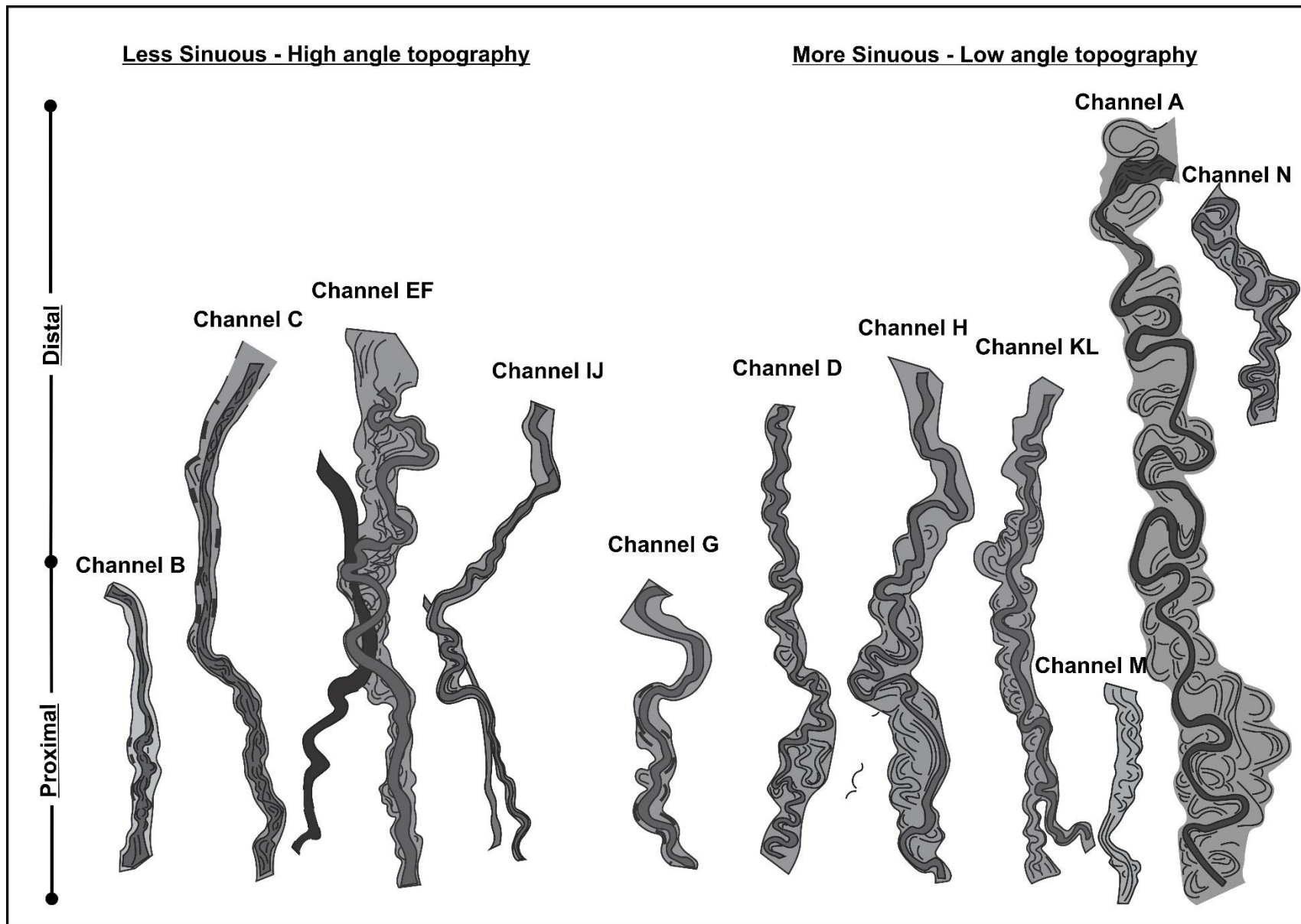


**Figure 18.** Sinuosity with interpretation of relative topography and channel's segments in the studied area within the Clifdenian-Tongaporutuan interval of the southern Taranaki Basin.

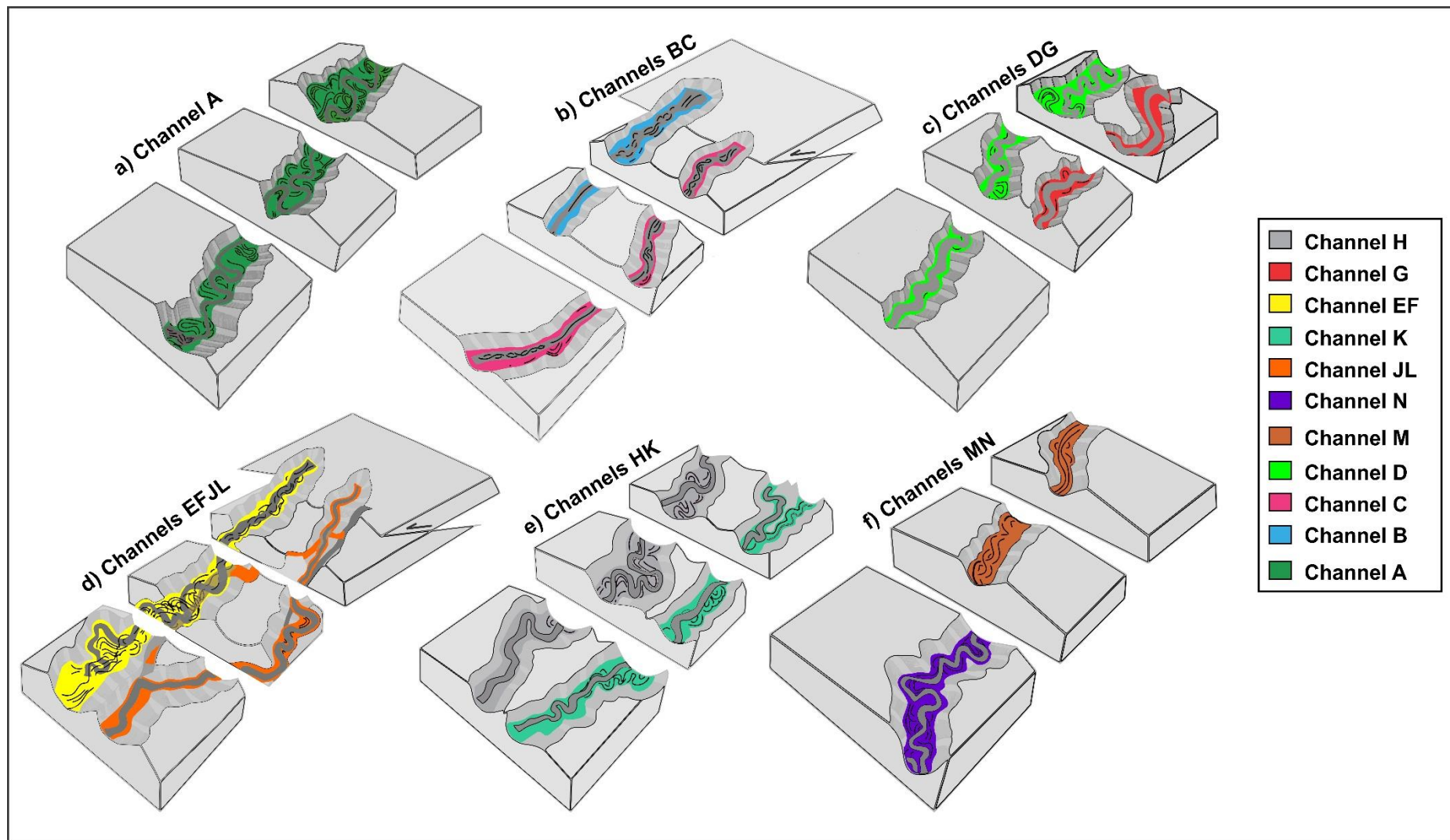
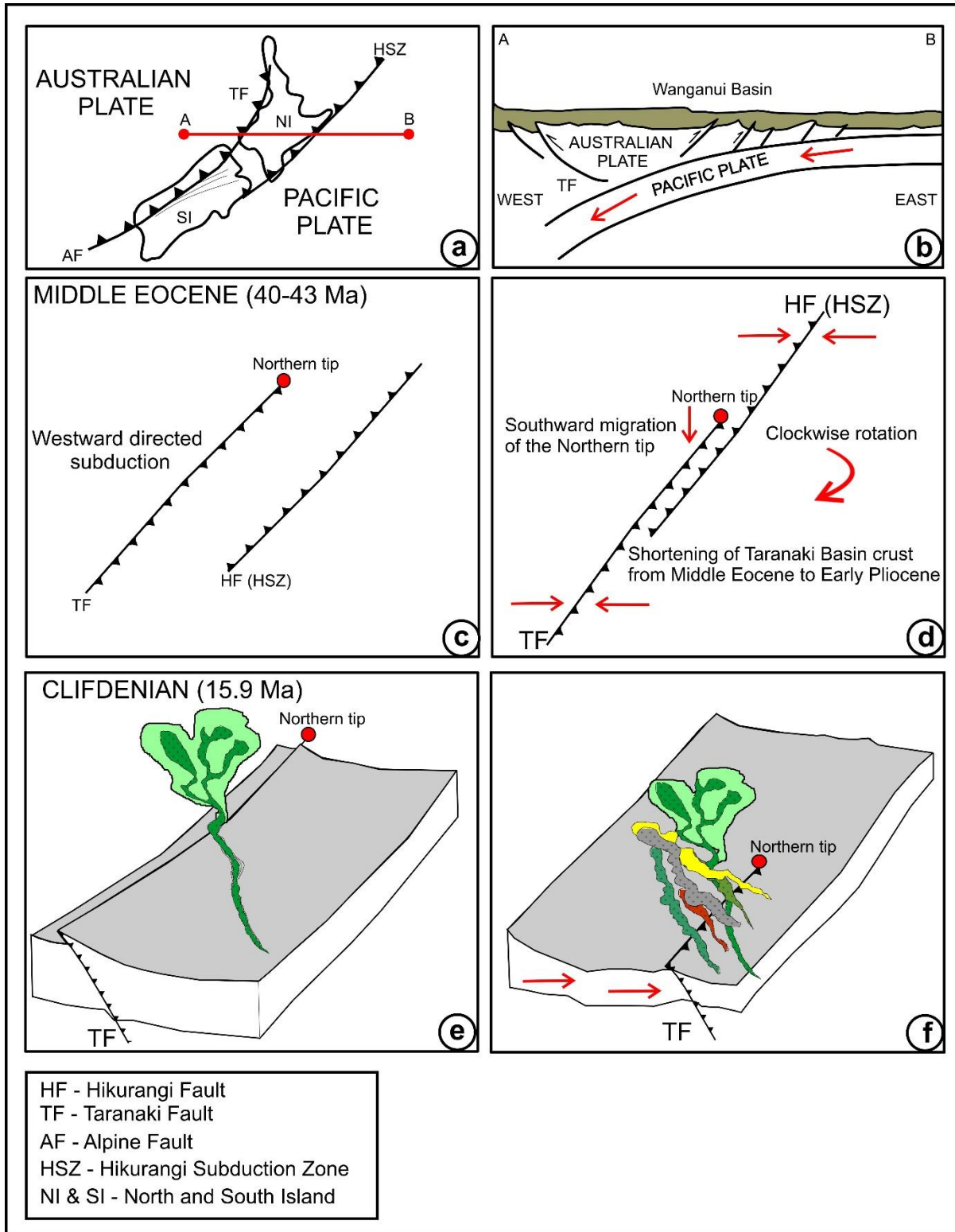


**Figure 19.** Depositional model of the submarine channel system in the studied area within the Clifdenian-Tongaporutuan interval of the southern Taranaki Basin.



3 **Figure 20.** Conceptual diagram showing the temporal and spatial evolution of submarine  
 4 channels within the Clifdenian-Tongaporutuan interval of the southern Taranaki Basin.

